ACS NANO

www.acsnano.org

ARTICLE

Structure, Stability, and Reorganization of 0.5 L_0 Topography in Block Copolymer Thin Films

Michael J. Maher,[†,⊥,▼] Jeffrey L. Self,[‡,§,▼] Pawel Stasiak,[∥,▼] Gregory Blachut,[‡] Christopher J. Ellison,[*,‡,⊥] Mark W. Matsen,[*,#] Christopher M. Bates,[*,¶,△] and C. Grant Willson[*,†,‡]

[†]Department of Chemistry and [‡]McKetta Department of Chemical Engineering, The University of Texas at Austin, Austin, Texas 78712, United States

[§]Department of Chemistry, [¶]Materials Department, and [△]Department of Chemical Engineering, University of California, Santa Barbara, California 93106, United States

[∥]Department of Mathematics & Statistics, University of Reading, Reading RG6 6AX, United Kingdom

[⊥]Department of Chemical Engineering and Materials Science, University of Minnesota, Minneapolis, Minnesota 55455, United States

[#]Department of Chemical Engineering, Department of Physics & Astronomy, Waterloo Institute for Nanotechnology, University of Waterloo, Waterloo, Ontario N2L 3G1, Canada

Supporting Information

ABSTRACT: The structure, stability, and reorganization of lamella-forming block copolymer thin film surface topography ("islands" and "holes") were studied under boundary conditions driving the formation of 0.5 L_0 thick structures at short thermal annealing times. Self-consistent field theory predicts that the presence of one perfectly neutral surface renders 0.5 L_0 topography thermodynamically stable relative to 1 L_0 thick features, in agreement with previous experimental observations. The calculated through-film structures match cross-sectional scanning electron micrographs, collectively demonstrating the pinning of edge dislocations at the neutral surface. Remarkably, near-neutral surface compositions exhibit 0.5 L_0 topography metastability upon extended thermal treatment, slowly transitioning to 1 L_0 islands or holes as evidenced by optical and atomic force microscopy. Surface restructuring is rationalized by invoking commensurability effects imposed by slightly preferential surfaces. The results described herein clarify the impact of interfacial interactions on block copolymer self-assembly and solidify an understanding of 0.5 L_0 topography, which is frequently used to determine neutral surface compositions of considerable importance to contemporary technological applications.

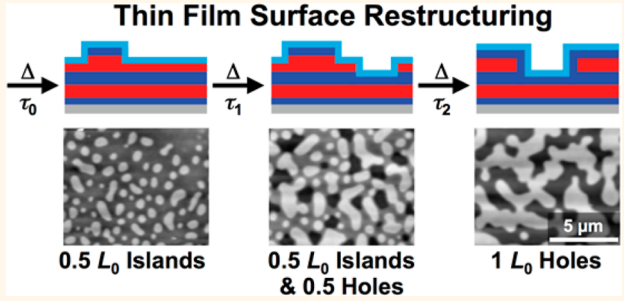

KEYWORDS: *block copolymers, self-assembly, islands, holes, terracing, surface reconstruction, SCFT, thin films*

Surface topography formed in block copolymer (BCP) thin films depends upon the nature of the interactions at the substrate and top surfaces.[1−4] When BCP lamellae orient parallel to the substrate, classic "island" and "hole" structures that adopt 1 L_0 height or depth form from initially incommensurate film thicknesses,[5,6] the definition of which depends on surface boundary conditions. When both surfaces display affinity for the same block ("symmetric wetting"), BCP films preferentially adopt commensurate $t = nL_0$ film thicknesses and avoid incommensurate thicknesses $(n + 0.5)L_0$; islands form when $n < t_0/L_0 < (n + 0.5)$, and holes form when $(n + 0.5) < t_0/L_0 < (n + 1)$. (Note the distinction between t_0, the as-cast film thickness, and t, the film thickness adopted after annealing; n is an integer, and L_0 is the bulk equilibrium domain spacing.) In contrast, the use of two surfaces that favor interaction with different blocks ("asymmetric wetting") produces commensurability at $t = (n + 0.5)L_0$ and incommensurability at $t = nL_0$; holes form when $n < t_0/L_0 < (n + 0.5)$, and islands form when $(n + 0.5) < t_0/L_0 < (n + 1)$. Recently, sufficiently thin films (roughly $t_0 \leq 3\ L_0$) confined by a single ostensibly neutral surface and a highly preferential surface (in either possible permutation) have been demonstrated to generate surface topography characterized by 0.5 L_0 height or depth and commensurability conditions including both $t = nL_0$ and $t = (n + 0.5)L_0$.[7] These relaxed commensurability constraints create an additional switch between topography at $t_0 = (n \pm 0.25)L_0$; "half-height" islands form when $n < t_0/L_0 < (n + 0.25)$ and $(n + 0.5) < t_0/L_0 < (n + 0.75)$, while "half-depth" holes form when $(n + 0.25) < t_0/L_0 <$

Received: August 10, 2016
Accepted: October 27, 2016
Published: October 27, 2016

DOI: 10.1021/acsnano.6b05390
ACS Nano 2016, 10, 10152−10160

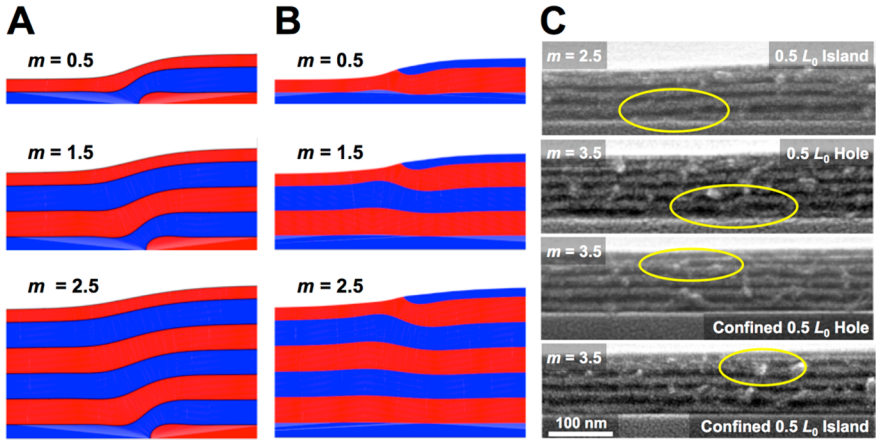

Figure 1. (A,B) Simulated step edges between films with m and m + 0.5 lamellae (*i.e.*, 0.5 L_0 topography) generated with f_A = 0.5 using (A) a neutral substrate surface and preferential top surface and (B) a preferential substrate surface and neutral top surface. The red and blue blocks correspond to PTMSS and PS, respectively. (C) Cross-sectional SEMs lightly etched side-on and coated top-down with Au/Pd (<3 nm) to accentuate contrast between PS (dark) and PTMSS (light). Top coats were not removed from confined samples prior to imaging. Edge dislocation defects are highlighted by yellow circles.

$(n + 0.5)$ and $(n + 0.75) < t_0/L_0 < (n + 1)$. The formation of these 0.5 L_0 structures, coupled with the addition of distinct commensurability conditions not seen with 1 L_0 structures, provides a particularly easy methodology for screening neutral surface compositions.[8]

Here, we address both the structure and stability of 0.5 L_0 topography in thin films (t_0 < 3 L_0) through a combination of theory and experiment. This report is organized into three sections: (i) the through-film configuration of 0.5 L_0 topography as evidenced by self-consistent field theory (SCFT) calculations and cross-sectional scanning electron microscopy (SEM), (ii) the thermodynamic (meta)stability of 0.5 L_0 topography in the presence of one preferential surface paired with either a perfectly neutral surface or a near-neutral (slightly preferential) surface, and (iii) the restructuring mechanism that transitions the film from metastable 0.5 L_0 to stable 1 L_0 topography in the latter case of (ii). These topics are extensively interrogated with experiments exhaustively spanning variable space including wetting conditions and film thickness. Details concerning the poly(styrene-*block*-4-trimethylsilylstyrene) block copolymer (PS–PTMSS, L_0 = 22 nm), surfaces, and simulations subsequently elaborated are provided in the Materials and Methods section along with the Supporting Information. The fundamental insights delivered herein significantly deepen our understanding of block copolymer thin film self-assembly.

RESULTS

Structure. SCFT was used to simulate the structure of symmetric AB diblock copolymer thin films confined by one preferential surface and one neutral surface; both permutations were studied (preferential top/neutral bottom and neutral top/preferential bottom) to emulate analogous experiments utilizing either a free surface or polymeric top coat.[7,8] Figure 1A,B reports results obtained for a variety of as-cast thicknesses ranging from t_0 = 0.5–2.5 L_0, where $m \equiv t/L_0$ is defined with the thinner t value adopted after annealing. Half topography is clearly formed for each film thickness, with both blocks contacting the neutral surface and a single block wetting the preferential surface. Similar data are also produced with other values of m and f_A (Figures S1 and S2). The neutral surface visibly pins the edge dislocation in either case, verifying previous speculative illustrations.[7,8] Figure 1C shows select corresponding cross-sectional SEMs that are fully consistent with this prediction; the edge dislocation is never found within the interior of the film and is only located against the neutral surface, either top or bottom. (Experimental difficulties acquiring complementary data on thinner films prevent us from reporting samples with m < 2.5, but all indications suggest comparable disposition.) The edge dislocation observed with 0.5 L_0 topography fundamentally differentiates the through-film structure compared to 1 L_0 islands and holes formed by two preferential interfaces. In the latter case, the defect is embedded within the interior of the film (Figures S3 and S4),[9−12] adopting a location determined by a delicate balance between surface field strength, commensurability, film thickness, and block copolymer attributes like volume fraction. Relatively thick films annealed with only one neutral surface experimentally yield mixed orientations as a function of through-film position (Figure S5), with perpendicular features contacting the neutral surface spatially transforming into parallel features induced by a single block wetting the preferential surface. The exact t_0 differentiating the 0.5 L_0 topography and mixed morphology regimes was not investigated, but the cross-sectional micrographs are in qualitative agreement with thick films previously studied.[13,14]

Stability. The SCFT predicts that the equilibrium coexistence between terraces separated by 0.5 L_0 is only possible for a perfectly neutral surface.[15] Given that the surface preference can never be precisely zero in an actual experiment, this begs the question of how the 0.5 L_0 topography would ever occur. The explanation has to do with kinetics. Since the equilibrium terrace heights are separated by first-order transitions and the topography is stable with respect to small fluctuations, the phase separation into coexisting terraces will occur by the classical nucleation and growth mechanism. As such, the formation (*i.e.*, nucleation) of islands or holes involves overcoming an energy barrier. A simple calculation (see Supporting Information Figure S6 and associated text) predicts that the relative barrier heights, $E_{B,0.5}$ and $E_{B,1}$, for nucleating 0.5 L_0 and 1 L_0 structures, respectively, on a neutral surface are given by

DOI: 10.1021/acsnano.6b05390
ACS Nano 2016, 10, 10152–10160

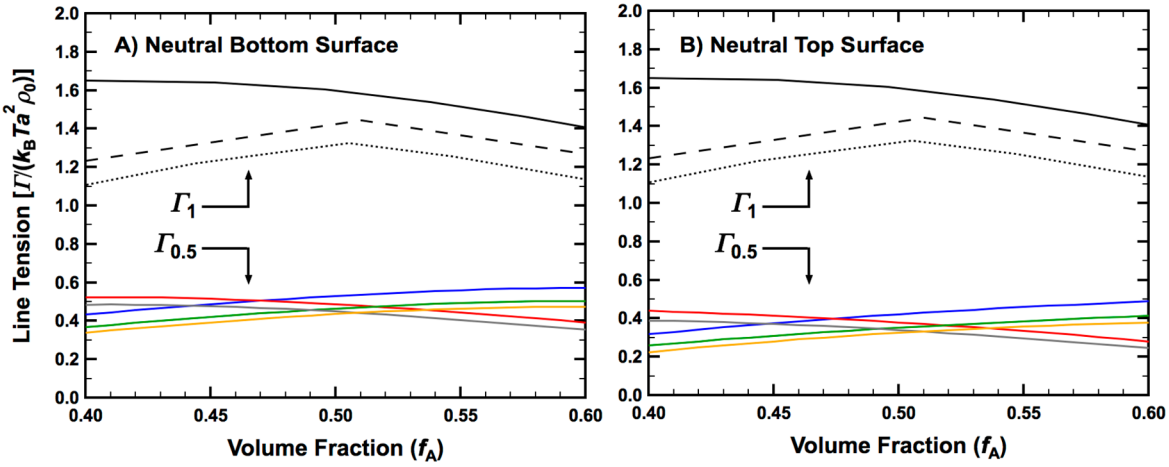

Figure 2. Line tensions of 0.5 L_0 (colored curves) and 1 L_0 (black curves) step edges calculated with SCFT for (a) a neutral substrate with preferential free surface and (b) a preferential substrate with a neutral top surface. The blue, red, green, gray, and yellow curves correspond to m = 0.5, 1.0, 1.5, 2.0, and 2.5, respectively, and the solid, dashed, and dotted black curves correspond to m = 0.5, 1.0, and 1.5, respectively. The latter curves are adapted from ref 12.

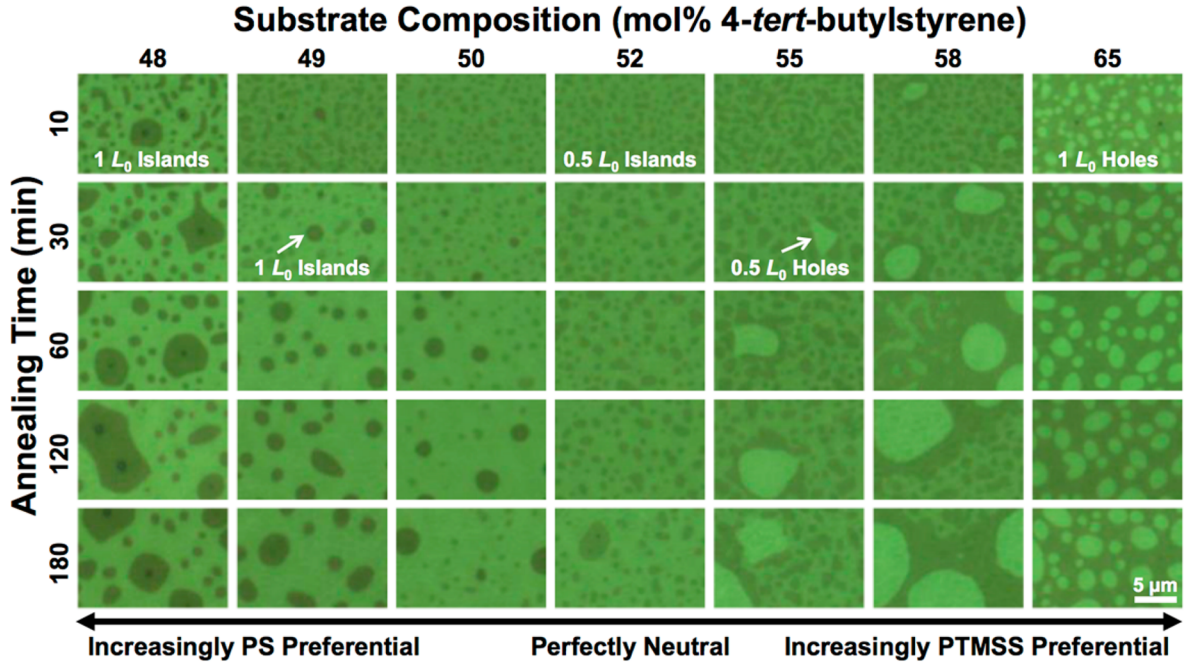

Figure 3. Optical micrographs demonstrate that topographic formation (t_0 = 1.65 L_0, annealed at 180 °C) and stability depend on substrate surface composition. See the Supporting Information for details on the blends used to tune composition. The scale bar is valid for all micrographs.

$$\frac{E_{B,0.5}}{E_{B,1}} = 2\left(\frac{\Gamma_{0.5}}{\Gamma_1}\right)^2$$

where $\Gamma_{0.5}$ and Γ_1 are the line tensions of 0.5 L_0 and 1 L_0 step edges, respectively. The factor of 2 comes from the fact that, for a given volume of material, the shorter 0.5 L_0 islands (or shallower 0.5 L_0 holes) will occupy twice the area of their 1 L_0 counterparts. Thus, their step edges will be longer, which impedes their nucleation. However, our SCFT predictions for the line tensions in Figure 2 show that $\Gamma_{0.5} \approx 0.3\ \Gamma_1$, which is more than enough to compensate for the factor 2 making the nucleation of 0.5 L_0 islands (or holes) far faster than their 1 L_0 counterparts. This conclusion holds for different film thickness, m, different diblock compositions, f_A, and regardless of whether or not it is the substrate or free surface that is neutral. Of course, the equilibrium film thicknesses are actually separated by L_0, and so the initial 0.5 L_0 topography should eventually switch to 1 L_0 topography.

Metastability. PS–PTMSS (t_0 = 1.65 L_0) was annealed at 180 °C for various times on substrate surfaces comprising cross-linked blends of poly(4-*tert*-butylstyrene-*random*-methyl methacrylate-*random*-4-vinylbenzylazide) (PtBS-*r*-PMMA-*r*-PVBzAz) containing different constituent ratios. (The free surface is highly PTMSS preferential in these experiments.) Optical micrographs (Figure 3) reveal that the resulting block copolymer topography is highly dependent on surface composition. The two extremes, 48 and 65 mol % of PtBS, are clearly preferential for PS and PTMSS blocks, respectively, as deduced from the formation of stable 1 L_0 islands and holes.

DOI: 10.1021/acsnano.6b05390
ACS Nano 2016, 10, 10152–10160

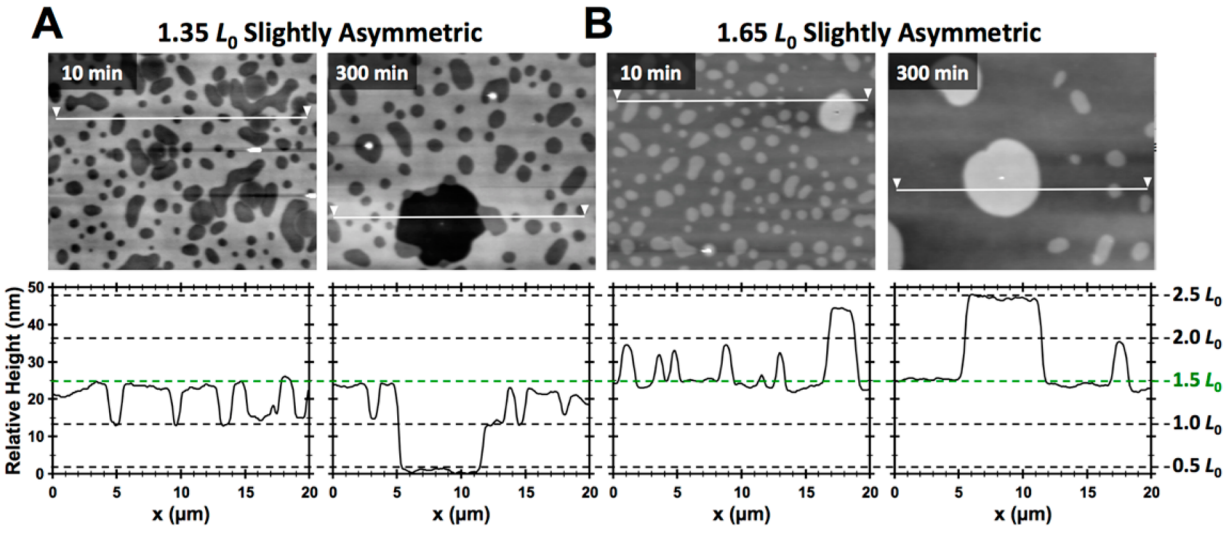

Figure 4. PS−PTMSS annealed at 180 °C for various times on a near-neutral substrate surface with air at the free surface.

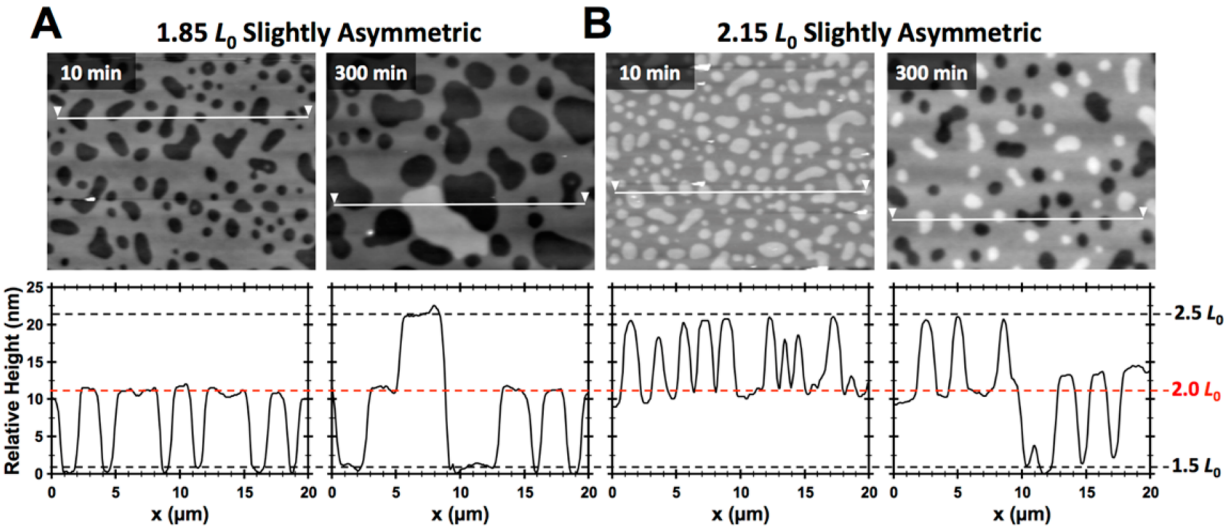

Figure 5. PS−PTMSS annealed at 180 °C for various times on a near-neutral substrate surface with air at the free surface.

A composition intermediate to the two extremes (52 mol %) is seemingly neutral as evidenced by the formation of stable 0.5 L_0 islands at all annealing times (10−180 min), in agreement with the theory presented in the previous section of this article. Remarkably, compositions skewed slightly away from neutral toward preferential interactions (49, 50, 55, and 58 mol %) exhibit markedly different behavior. Early times (*ca.* 10 min) generate mostly half islands as expected for a single neutral surface, but heterogeneous secondary nucleation and coalescence of different topography competes during extended annealing, causing significant overall surface restructuring. (Additional supplemental optical micrographs are shown in Figures S7 and S8.) This thermodynamic metastability on near-neutral surfaces and the factors governing reorganization were subsequently analyzed in detail; the origin of the labels superposed on Figure 3, defined relative to the initially formed matrix thickness coincident with 0.5 L_0 topography nucleation, will become clear in the next section. Additional analysis is available in the Discussion.

Surface Restructuring. The origins of metastability and the type of topography formed during secondary nucleation were studied with two boundary conditions: (1) slightly asymmetric wetting imposed by a moderately PS preferential substrate paired with air or vacuum at the free surface (which are both highly PTMSS preferential), and (2) slightly symmetric wetting arising from a preferential substrate (cross-linked PS homopolymer) with a moderately PS preferential top coat.

Asymmetric Wetting. PS−PTMSS with t_0 = 1.35 L_0 generates half holes in 10 min, comprising a matrix at t = 1.5 L_0 and troughs at t = 1 L_0 (Figure 4A). Continued thermal annealing (300 min total) further nucleates 1 L_0 deep holes with a matrix still at t = 1.5 L_0 and troughs now occupying t = 0.5 L_0. Figure 4B shows analogous experiments conducted with t_0 = 1.65 L_0; half islands form, again with a matrix residing at t = 1.5 L_0 and apexes now at t = 2 L_0. The sample annealed for 10 min already contains a low areal density of 1 L_0 structures spanning t = 1.5−2.5 L_0, which significantly grow in both areal density and footprint after extended annealing to 300 min.

Both t_0 = 1.85 L_0 and 2.15 L_0 as-cast thicknesses also quickly form 0.5 L_0 topography that slowly reconfigures into 1 L_0 topography (Figure 5). Over time, the t_0 = 1.85 L_0 sample originally containing only half holes further nucleates half islands from the matrix region that span t = 2−2.5 L_0

DOI: 10.1021/acsnano.6b05390
ACS Nano 2016, 10, 10152−10160

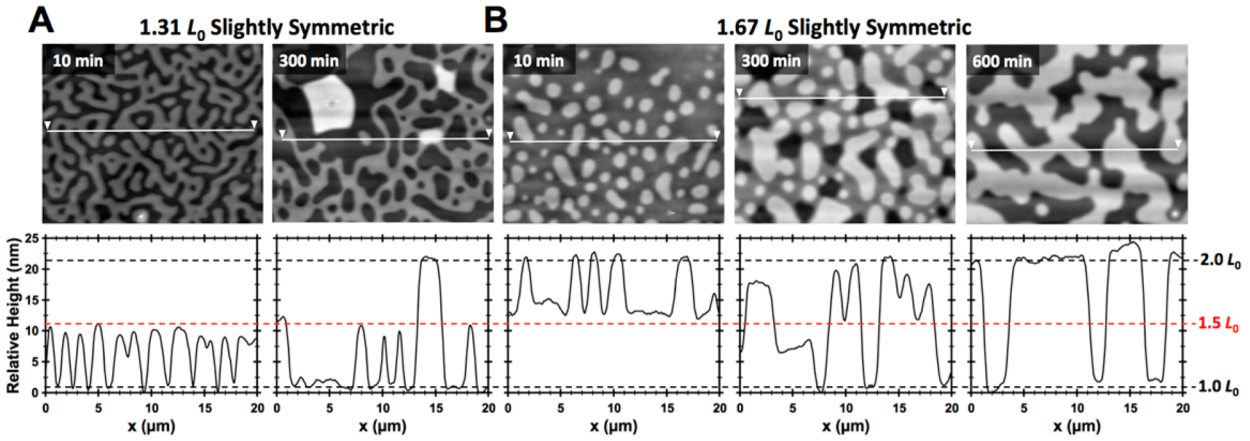

Figure 6. PS−PTMSS annealed at 180 °C between a PS homopolymer substrate and a near-neutral top coat.

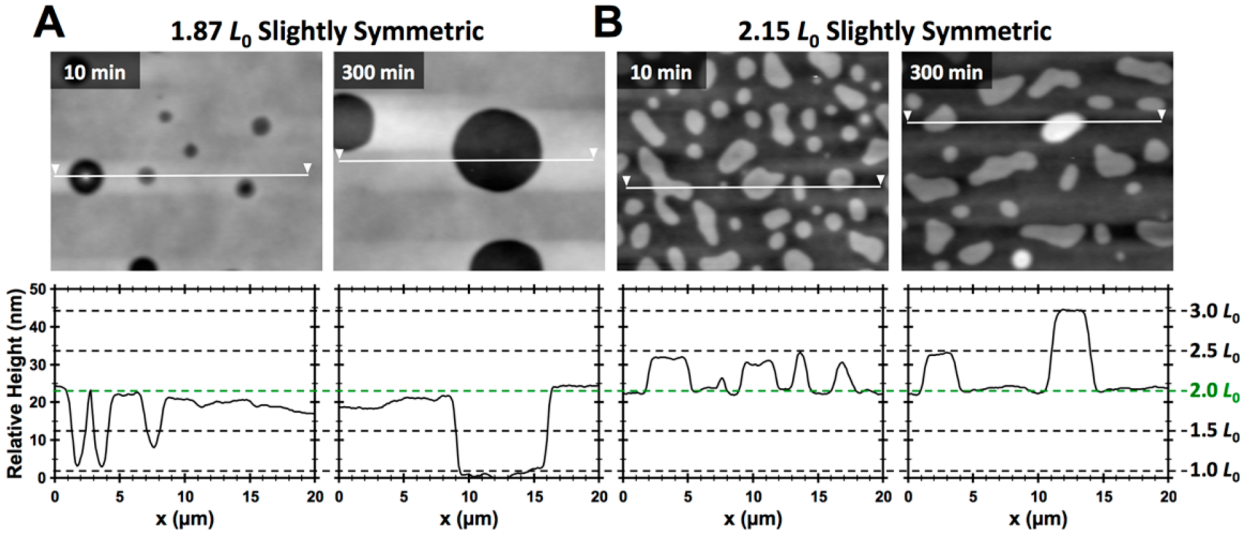

Figure 7. PTMSS−PS annealed at 180 °C between a PS homopolymer substrate and a near-neutral top coat.

thicknesses. The t_0 = 2.15 L_0 sample, initially displaying half islands, also nucleates the opposite type of half topography (0.5 L_0 holes) from the matrix region after 300 min annealing. For both samples, the mixture of nominally two different 0.5 L_0 structures actually represents a transient state captured during surface reconstruction that will eventually yield 1 L_0 topography spanning t = 1.5−2.5 L_0 absolute film thicknesses. Further evidence supporting this conclusion is provided below. The 1 L_0 topography formed after extended thermal annealing for all four samples shown in Figures 4 and 5 is consistent with asymmetric wetting exhibiting commensurability at $t = (n + 0.5)L_0$; 1 L_0 thick topography resides at t = 0.5, 1.5, and 2.5 L_0 depending on the as-cast t_0. Additional film thicknesses (t_0 = 1.17, 2.35, 2.65, and 2.85 L_0; see Figures S9−S12) are fully consistent with the above interpretations.

Symmetric Wetting. Figures 6 and 7 show experiments conducted with a PS preferential substrate surface and a near-neutral top coat. At short annealing times, t_0 = 1.31 L_0 forms exclusively 0.5 L_0 holes. (Note that the two-dimensional pattern looks nearly bicontinuous due to the large Δt_0 relative to the t = 1.5 L_0 commensurate condition.) After extended annealing, 0.5 L_0 islands nucleate from the t = 1.5 L_0 matrix. Evidence that these structures, in fact, represent 1 L_0 topography spanning t = 1−2 L_0 can be found by inspecting the t_0 = 1.67 L_0 sample (Figure 6B). At short annealing times (10 min), half islands form with a matrix at t = 1.5 L_0 and apexes at t = 2 L_0, consistent with nonpreferential wetting at the top interface. Further annealing (300 min) of the same sample nucleates half hole-like features from the matrix, with troughs residing at t = 1 L_0 thickness and continued annealing to 600 min completely eliminates the matrix originally residing at t = 1.5 L_0; the film now contains only 1 L_0 thick topography spanning t = 1−2 L_0 absolute film thicknesses. The final structures formed are thus consistent with full holes as expected for $1.5 < t_0/L_0 < 2$ with symmetric boundary conditions characterized by commensurability at $t = nL_0$. Not all films fully transitioned from kinetically formed half structures to thermodynamically stable 1 L_0 topography after 600 min annealing, but all films at least partially reconstructed after modest (300 min) thermal treatment. We conclude that most data reported herein at 300 min represent a fleeting snapshot captured during surface reconstruction; presumably given enough time, these samples would fully transition to 1 L_0 topography as observed with t_0 = 1.67 L_0.

A t_0 = 1.87 L_0 sample quickly forms a mixture of approximately 0.5 L_0 and 1 L_0 topography after 10 min annealing (Figure 7A). After 300 min, the troughs of the 0.5 L_0 features decrease in thickness, fully transforming into 1 L_0 holes traversing t = 1−2 L_0. Likewise, the half islands generated with t_0 = 2.15 L_0 (Figure 7B) begin to coexist with 1 L_0 islands upon

DOI: 10.1021/acsnano.6b05390
ACS Nano 2016, 10, 10152−10160

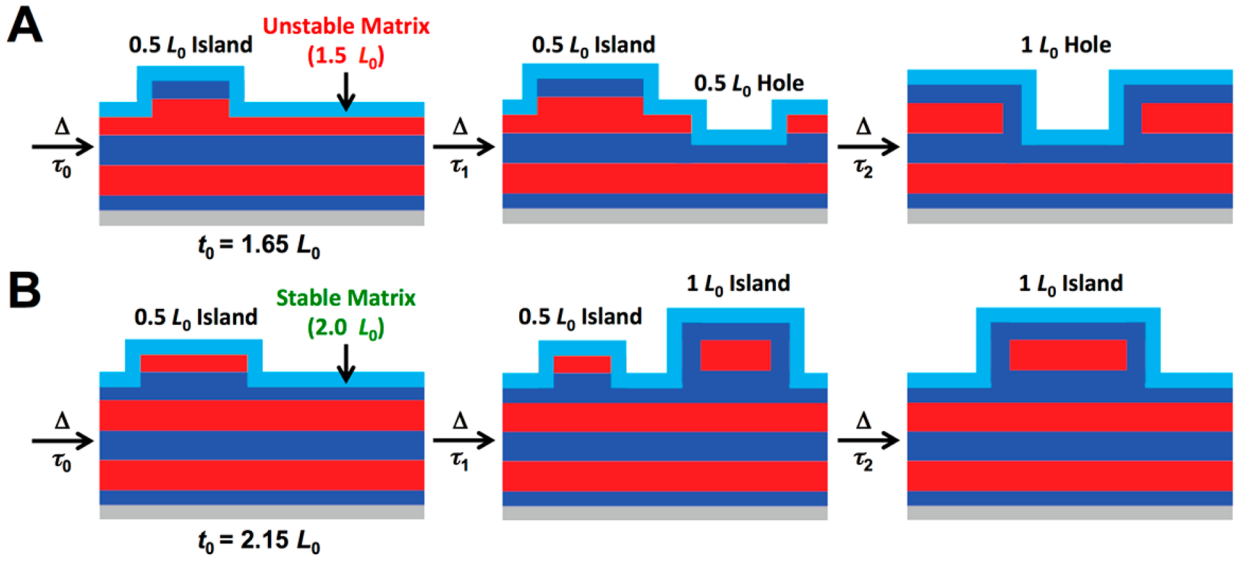

Figure 8. Surface reconstruction as a function of time for a preferential substrate and near-neutral top coat (overall, slightly symmetric wetting) with as-cast BCP thickness (A) t_0 = 1.65 L_0 and (B) t_0 = 2.15 L_0.

extended annealing. Additional samples with t_0 = 1.16, 2.37, 2.63, and 2.82 L_0 are provided in the Supporting Information (Figures S13–S16) and generally reinforce the behavior observed in Figures 6 and 7.

DISCUSSION

Previous studies on 0.5 L_0 topography specifically targeted the use of a single "perfectly neutral" surface (characterized by exactly balanced interfacial interactions with each block, $\Delta\gamma \equiv \gamma_{AS} - \gamma_{BS} = 0$) to generate half structures.[7,8] While theory now confirms that half islands and holes are indeed thermodynamically stable in the presence of a single perfectly neutral interface, achieving true surface neutrality with real materials is technically impossible. Experimentally, interactions at both the bottom[16−18] and top[8,19] surfaces are conveniently tuned with polymer composition.[16] The experiments described in Figures 3−7 demonstrate that 0.5 L_0 topography still kinetically forms on surface compositions that are near-neutral, but thermodynamic metastability triggers surface reconstruction upon extended annealing. Quantifying surface neutrality (*i.e.*, measuring $|\gamma_s - \gamma_{neutral}|$, where γ_s is the surface tension of the given surface and $\gamma_{neutral}$ is the surface tension of a perfectly neutral surface) with the precision necessary to differentiate small changes in surface composition is currently impossible, but Figure 3 provides qualitative insight into the breadth of the perfectly and near-neutral composition windows. Care should be taken not to overinterpret the absolute magnitude of the differences; assuming surface energy scales linearly with polymer composition, the rate of change ($d\gamma/dc$, where c is surface treatment composition) depends on the surface energy of the constituent monomeric components ($\gamma_{c=0}$ and $\gamma_{c=1}$). BCP attributes such as relative volume fraction and the block−block interfacial tension ($\gamma_{AB} \sim \chi^{-0.5}$) may also contribute, although such conjectures remain speculative and currently unsubstantiated. The optical micrographs in Figure 3 do provide evidence that the time scale associated with nucleation (τ_1) and corresponding growth (τ_2) of secondary islands and holes after initial kinetic formation of 0.5 L_0 topography (τ_0) correlates with the differential surface composition relative to perfect neutrality ($\tau_{1,2} \sim \Delta c^{\beta} = |c_s - c_{neutral}|^{\beta}$). For instance, supposing a neutral surface treatment composition $c_{neutral} \approx 52$ mol % of PtBS, c_s = 50 and 55 mol % show minimal evidence of secondary nucleation after 10 min, which begins to emerge at only *ca.* 30 min. In contrast, surfaces with 49 and 58 mol % already generate a low density of secondary nuclei after 10 min, while surfaces far from neutral compositions entirely forego nucleation of metastable 0.5 L_0 topography even at short times in favor of classical 1 L_0 islands (48 mol %) and holes (65 mol %). Extracting the exact functional form of $\tau_{1,2}$, including any exponential dependence (β), would require additional kinetic studies beyond the scope of this report. Given the apparent τ dependence for obliteration of kinetically formed 0.5 L_0 topography, even definitive proclamation of perfect neutrality at $c_{neutral}$ = 52 mol % is tenuous at best because lengthened annealing may ultimately yield surface reconfiguration.

At least some near-neutral surface compositions displaying thermodynamic metastability are for all practical purposes "neutral" in the sense that they successfully orient block copolymer lamellae perpendicular to the substrate when coupled with a second neutral surface.[20] Such orientation can only be achieved in the presence of two sufficiently neutral surfaces.[21,22] Potentially subtle distinction between perfectly neutral, near-neutral, and preferential surfaces, straddling compositions capable and incapable of orienting BCPs, is critical for interfacial design. The surface restructuring mechanism studied in detail herein portends a trivial experimental approach that delineates perfectly neutral and near-neutral surfaces. This demarcation might gain additional importance in the continued race toward high-χ BCPs for lithographic applications.[23]

The surface reconstruction mechanism can be rationalized with commensurability effects established by surface boundary conditions operating on kinetically formed 0.5 L_0 topography. A single near-neutral surface unambiguously generates 0.5 L_0 topography at short annealing times (τ_0), as evidenced by Figures 3−7 and previous literature reports.[7,8] Subsequent restructuring depends on both the commensurability of the resulting matrix and the thickness occupied by half feature apexes/troughs (illustrated with select examples in Figure 8). For circumstances involving a matrix that is commensurate with

DOI: 10.1021/acsnano.6b05390
ACS Nano 2016, 10, 10152−10160

the boundary conditions (*e.g.*, Figures 4 and 7), 0.5 L_0 topography transitions directly into 1 L_0 topography either *via* mass transfer into (or out of) the existing 0.5 L_0 structures or by direct nucleation of full features from the matrix (with a corresponding reduction of each half feature area footprint). Half structures thus appear to directly morph into full features during annealing, as depicted in Figure 8B. In contrast, when the matrix initially adopts a thickness that is incommensurate with the boundary conditions (*e.g.*, Figures 5 and 6), it nucleates the opposite 0.5 L_0 topography while simultaneously maintaining the original half features (Figure 8A). Pairs of 0.5 islands and holes eventually agglomerate, concurrent with annihilation of the matrix, to eventually yield 1 L_0 topography terminating at thicknesses fully commensurate with the surface-imposed boundary conditions (Figure 6B). Note that Figure 8 depicts a preferential substrate and near-neutral top coat in direct analogy to Figure 6B; see Figure S17 for the opposite illustration with a preferential top surface and near-neutral substrate. We are unaware of any analogous studies describing the reorganization of 1 L_0 topography driven by changes in surface wetting, although the results reported herein indicate such reconstruction may be possible with suitable materials that controllably alter preferential interfacial interactions. Top coats might facilitate the prerequisite dynamic wettability since they are inherently strippable using solvent without damaging the underlying BCP film. Alternatively, photoinduced switching of surface wettability may provide similar control *via* a complementary mechanism.[24,25]

A brief discussion is warranted regarding the confinement regime accessed with maleic anhydride top coats. Koneripalli *et al.* have previously studied block copolymers sandwiched between a solid substrate and polystyrene top coat.[26] Notably, with their materials, island and hole formation is suppressed in favor of stretched or compressed block copolymer domains that uniformly cover the as-cast thickness with an integral number of periods. The underlying physical characteristics that distinguish polystyrene from maleic anhydride top coats are still not fully understood. Both "hard" polystyrene top coat ($T_g \approx 100$ °C) and apparently "soft" maleic anhydride top coats ($T_g \approx 200$ °C) are nominally glassy under the selected annealing conditions (which differ between reports) with presumably typical elastic moduli *ca.* 1 GPa. (Note that we have not measured the mechanical properties of maleic anhydride copolymers.) We speculate that the important difference may be related to the presence of trimethylammonium ions. For solubility reasons, our top coats are cast as trimethylammonium salts, which upon annealing ring-close to form maleic anhydride with concomitant liberation of water and trimethylamine gas,[8] likely forming internal voids within the top coat. Our working hypothesis is that these voids increase free volume, transforming the top coat from a glassy to melt state. Although we are not absolutely certain of this, there is no doubt these polymers can be considered "soft" for all practical purposes on the time scale of our experiments. Maleic anhydride top coats unambiguously contort to reveal block copolymer surface topography, which is readily interpreted to extract surface wetting information.[8] In contrast, hard materials like polystyrene[26] and SiO_x[27] are incapable of deformation and consequently perturb the bulk block copolymer periodicity in lieu of island and hole formation. We conclude that the regime probed herein, using the nomenclature of Koneripalli, must be considered "pseudoconfinement", in analogy to annealing with a free surface (*e.g.*, air or vacuum). Although surprising, to date, we have identified no significant differences between the surface topography produced from a block copolymer annealed under a maleic anhydride top coat or a free surface. Since the present paper focuses on wetting effects and associated surface reconfiguration on near-neutral surfaces, a detailed physical model encapsulating all of the aforementioned factors governing top coat pseudoconfinement is well beyond the intended scope of this report.

CONCLUSION

The through-film structure, thermodynamic (meta)stability, and reconfiguration mechanism of 0.5 L_0 block copolymer topography formed in the presence of one neutral and one preferential interface were studied through a combination of experiment and self-consistent field theory. Kinetic formation of 0.5 L_0 features at short annealing times is driven by significantly reduced line tension relative to 1 L_0 structures. The edge dislocation necessarily generated by 0.5 L_0 topography is pinned to the neutral or near-neutral interface (either top or bottom), in contrast to 1 L_0 features in which defects are generally embedded within the interior of the film. While the utilization of a single perfectly neutral surface renders 0.5 L_0 topography thermodynamically stable, a single near-neutral surface imparts metastability relative to 1 L_0 structures. Half features correspondingly reconstruct during annealing to nucleate and grow topography that ultimately transforms into 1 L_0 islands or holes, determined by surface boundary conditions. Secondary nucleation time scales appear to be correlated with surface composition, whereby nearly neutral materials maintain metastable half features longer than surfaces skewed more preferential. The mechanism of surface reconstruction depends sensitively on film thickness and commensurability.

MATERIALS AND METHODS

Experiment. The BCP discussed herein, poly(styrene-*block*-4-trimethylsilylstyrene) (PS−PTMSS) with L_0 = 22 nm, typifies a convenient model system due to inherently PTMSS preferential interactions at the free surface[28] which are readily modifiable with top coats.[8] We note in passing that silicon-containing BCPs including PS−PTMSS are also potentially useful for lithographic applications.[29−32] The influence of substrate composition on topographic metastability was studied with blends generated by mixing two poly(4-*tert*-butylstyrene-*random*-methyl methacrylate-*random*-4-vinylbenzylazide) PtBS-*r*-PMMA-*r*-PVBzAz copolymers in various ratios; see the Supporting Information for details. Restructuring mechanistic studies applied various combinations of surfaces to systematically vary thin film commensurability conditions. The surfaces used included (1) a PtBS-*r*-PMMA-*r*-PVBzAz near-neutral substrate surface treatment (slightly PS wetting) with 53 mol % of PtBS, 42 mol % of PMMA, 5 mol % of PVBzAz; (2) a near-neutral (slightly PS wetting) top coat, poly(styrene-*alt*-maleic anhydride)-*random*-poly(3,5-di-*tert*-butylstyrene-*alt*-maleic anhydride) (50 mol % of maleic anhydride, 20 mol % of 3,5-di-*tert*-butylstyrene, 30 mol % of styrene); and (3) a PS preferential substrate surface, poly(styrene-*random*-4-vinylbenzylazide) (95 mol % of PS, 5 mol % of PVBzAz). Synthetic details and characterization of these materials can be found in the Supporting Information and elsewhere.[8]

Theory. To model the terraces and the step edges between them, we use SCFT, which is regarded as the state-of-the-art for block copolymer melts.[33,34] SCFT has recently been used to provide what is undoubtedly the most accurate theoretical treatment of 1 L_0 step edges in block copolymer films.[12] Here, we use the same approach for the 0.5 L_0 step edges.

The diblock copolymers are modeled by flexible Gaussian chains of N_A A-type segments joined to N_B B-type segments. Both types of

DOI: 10.1021/acsnano.6b05390
ACS Nano 2016, 10, 10152−10160

segments are defined to occupy an equal volume of ρ_0^{-1} and assumed to have the same statistical segment length, a. The composition of the diblock is given by $f_A \equiv N_A/N$, where $N = N_A + N_B$. The immiscibility of the A and B segments is modeled by a point-like repulsion controlled by the standard Flory–Huggins interaction parameter, χ_{AB}. For flexible polymers, the *hard* substrate can be treated by imposing a reflecting boundary at $z = 0$.[34,35] As justified in ref 12, the *soft* free surface can be conveniently modeled by filling the space above the diblock copolymer film with homopolymers of infinite molecular weight. The tensions (*i.e.*, γ_{Ah} and γ_{Bh}) and affinity (*i.e.*, $\Delta\gamma = \gamma_{Ah} - \gamma_{Bh}$) of the free surface are controlled by introducing interactions between the homopolymer and the A and B diblock components with interaction parameters, χ_{Ah} and χ_{Bh}, respectively. Note that the top coats in our experiments actually involve two surfaces, one with the BCP and another with the air. However, for thin top coats of uniform thickness, both surfaces will have the same area and thus can be treated as a single surface with a net tension equal to the sum of the BCP/top coat and top coat/air surface tensions.

In SCFT, the molecular interactions experienced by the A, B, and homopolymer segments are approximated by mean fields, $w_A(\mathbf{r})$, $w_B(\mathbf{r})$, and $w_h(\mathbf{r})$, respectively. The calculation starts with appropriate initial guesses for the fields, where their minima correspond to the expected locations of the corresponding components. Given the fields, diffusion equations are solved for propagators from which the concentrations of the three components, $\phi_A(\mathbf{r})$, $\phi_B(\mathbf{r})$, and $\phi_h(\mathbf{r})$, are calculated. The fields are then adjusted iteratively until they satisfy the self-consistent conditions

$$w_A(\mathbf{r}) = \chi_{AB}N\phi_B(\mathbf{r}) + \chi_{Ah}N\phi_h(\mathbf{r}) + \xi(\mathbf{r})$$

$$w_B(\mathbf{r}) = \chi_{AB}N\phi_A(\mathbf{r}) + \chi_{Bh}N\phi_h(\mathbf{r}) + \xi(\mathbf{r})$$

$$w_h(\mathbf{r}) = \chi_{Ah}N\phi_A(\mathbf{r}) + \chi_{Bh}N\phi_B(\mathbf{r}) + \xi(\mathbf{r})$$

where $\xi(\mathbf{r})$ is a pressure field that enforces the incompressibility condition, $\phi_A(\mathbf{r}) + \phi_B(\mathbf{r}) + \phi_h(\mathbf{r}) = 1$. Once the solution is obtained, the domains of the film are defined according to the maximum concentration among $\phi_A(\mathbf{r})$, $\phi_B(\mathbf{r})$, and $\phi_h(\mathbf{r})$.

To calculate the equilibrium terraces, we solve the field equations for uniform solutions with different numbers of layers, where the fields and concentrations depend only on the z coordinate normal to the substrate. The free energy curves of the different film thicknesses exhibit a sequence of local minimums, and the first-order transitions between them are located by performing double-tangent constructions.[15] The step edge separating two coexisting terrace heights is obtained by simply allowing the fields to also vary in one of the lateral directions. In the case of 1 L_0 step edges, there is a metastable solution for each possible location of the dislocation within the film; the preferred stable location is the one that minimizes the free energy. For 0.5 L_0 step edges, however, the only physical solution is the one with a dislocation at the neutral surface. To obtain the line tension of the step edge, Γ, we calculate the free energy of the SCFT solution containing the step edge and subtract off the free energy of the coexisting uniform terraces with relative surface areas given by the lever rule of the double-tangent construction (see ref 12).

To model a neutral substrate and a preferential free surface, we set $\chi_{Ah}N = 30$ and $\chi_{Bh}N = 50$, which gives a surface affinity for the A component (representing PTMSS and denoted by red). For a preferential substrate and a neutral free surface, we set $\chi_{Ah}N = \chi_{Bh}N = 30$ and restrict our attention to morphologies where the B component (representing PS and denoted by blue) covers the entire substrate. In all cases, we fix $\chi_{AB}N = 20$, which corresponds to a block copolymer melt of intermediate segregation. The one shortcoming of the SCFT is that we cannot solve the field equations for realistic values of χ_{Ah} and χ_{Bh}, and consequentially, the step edges will be somewhat sharper than in experiment.[12] Although this will underestimate the line tensions, $\Gamma_{0.5}$ and Γ_1, of the 0.5 L_0 and 1 L_0 step edges, respectively, SCFT should still provide a reasonable prediction of their ratio, $\Gamma_{0.5}/\Gamma_1$.

ASSOCIATED CONTENT

Supporting Information

The Supporting Information is available free of charge on the ACS Publications website at DOI: 10.1021/acsnano.6b05390.

Detailed experimental procedures, mathematical model for island and hole nucleation, and Figures S1–S17 (PDF)

AUTHOR INFORMATION

Corresponding Authors

*E-mail: cellison@umn.edu.
*E-mail: mwmatsen@uwaterloo.ca.
*E-mail: bates@engr.ucsb.edu.
*E-mail: willson@che.utexas.edu.

Author Contributions

▼M.J.M., J.L.S., and P.S. contributed equally to this work.

Notes

The authors declare no competing financial interest.

ACKNOWLEDGMENTS

The authors thank Nissan Chemical Industries, Lam Research, the ASTC, and the National Science Foundation (Grants EECS-1120823 and EEC-1160494) for financial support. M.J.M. thanks the IBM Ph.D. Fellowship Program and the National Science Foundation Graduate Research Fellowship (Grant No. DGE-1110007) for financial support. M.J.M. thanks Elizabeth Lofano for assistance with cross-sectional SEM. G.B. thanks the Paul D. Meek Endowed Graduate Fellowship in Engineering for support. C.J.E. thanks the Welch Foundation (Grant No. F-1709) for partial financial support. C.M.B. thanks the University of California, Santa Barbara, for financial support. G.W. thanks the Rashid Engineering Regents Chair and the Welch Foundation (Grant No. F-1830) for partial financial support. Any opinions, findings, and conclusions or recommendations expressed in this material are those of the authors and do not necessarily reflect the views of the National Science Foundation or the sponsors.

REFERENCES

(1) Coulon, G.; Russell, T. P.; Deline, V. R.; Green, P. F. Surface-Induced Orientation of Symmetric, Diblock Copolymers: A Secondary Ion Mass-Spectrometry Study. *Macromolecules* **1989**, *22*, 2581–2589.

(2) Russell, T. P.; Coulon, G.; Deline, V. R.; Miller, D. C. Characteristics of the Surface-Induced Orientation for Symmetric Diblock PS/PMMA Copolymers. *Macromolecules* **1989**, *22*, 4600–4606.

(3) Mansky, P.; Russell, T. P.; Hawker, C. J.; Pitsikalis, M.; Mays, J. Ordered Diblock Copolymer Films on Random Copolymer Brushes. *Macromolecules* **1997**, *30*, 6810–6813.

(4) Peters, R. D.; Yang, X. M.; Kim, T. K.; Sohn, B. H.; Nealey, P. F. Using Self-Assembled Monolayers Exposed to X-Rays to Control the Wetting Behavior of Thin Films of Diblock Copolymers. *Langmuir* **2000**, *16*, 4625–4631.

(5) Coulon, G.; Ausserre, D.; Russell, T. P. Interference Microscopy on Thin Diblock Copolymer Films. *J. Phys. (Paris)* **1990**, *51*, 777–786.

(6) Ausserre, D.; Chatenay, D.; Coulon, G.; Collin, B. Growth of Two Dimensional Domains in Copolymer Thin Films. *J. Phys. (Paris)* **1990**, *51*, 2571–2580.

(7) Kim, S.; Bates, C. M.; Thio, A.; Cushen, J. D.; Ellison, C. J.; Willson, C. G.; Bates, F. S. Consequences of Surface Neutralization in Diblock Copolymer Thin Films. *ACS Nano* **2013**, *7*, 9905–9919.

(8) Maher, M. J.; Bates, C. M.; Blachut, G.; Sirard, S.; Self, J. L.; Carlson, M. C.; Dean, L. M.; Cushen, J. D.; Durand, W. J.; Hayes, C.

DOI: 10.1021/acsnano.6b05390
ACS Nano 2016, 10, 10152–10160

O.; Ellison, C. J.; Willson, C. G. Interfacial Design for Block Copolymer Thin Films. *Chem. Mater.* **2014**, *26*, 1471−1479.
(9) Turner, M. S.; Maaloum, M.; Ausserre, D.; Joanny, J. F.; Kunz, M. Edge Dislocations in Copolymer Lamellar Films. *J. Phys. II* **1994**, *4*, 689−702.
(10) Carvalho, B.; Thomas, E. Morphology of Steps in Terraced Block Copolymer Films. *Phys. Rev. Lett.* **1994**, *73*, 3321−3324.
(11) Liu, Y.; Rafailovich, M. H.; Sokolov, J.; Schwarz, S. A.; Bahal, S. Effects of Surface Tension on the Dislocation Structures of Diblock Copolymers. *Macromolecules* **1996**, *29*, 899−906.
(12) Stasiak, P.; McGraw, J. D.; Dalnoki-Veress, K.; Matsen, M. W. Step Edges in Thin Films of Lamellar-Forming Diblock Copolymer. *Macromolecules* **2012**, *45*, 9531−9538.
(13) Huang, E.; Pruzinsky, S.; Russell, T. P.; Mays, J.; Hawker, C. J. Neutrality Conditions for Block Copolymer Systems on Random Copolymer Brush Surfaces. *Macromolecules* **1999**, *32*, 5299−5303.
(14) Xu, T.; Hawker, C. J.; Russell, T. P. Interfacial Interaction Dependence of Microdomain Orientation in Diblock Copolymer Thin Films. *Macromolecules* **2005**, *38*, 2802−2805.
(15) Matsen, M. W. Thin Films of Block Copolymer. *J. Chem. Phys.* **1997**, *106*, 7781−7791.
(16) Mansky, P.; Liu, Y.; Huang, E.; Russell, T. P.; Hawker, C. Controlling Polymer-Surface Interactions with Random Copolymer Brushes. *Science* **1997**, *275*, 1458−1460.
(17) Ryu, D. Y.; Shin, K.; Drockenmuller, E.; Hawker, C. J.; Russell, T. P. A Generalized Approach to the Modification of Solid Surfaces. *Science* **2005**, *308*, 236−239.
(18) Bang, J.; Bae, J.; Löwenhielm, P.; Spiessberger, C.; Given-Beck, S. A.; Russell, T. P.; Hawker, C. J. Facile Routes to Patterned Surface Neutralization Layers for Block Copolymer Lithography. *Adv. Mater.* **2007**, *19*, 4552−4557.
(19) Bates, C. M.; Seshimo, T.; Maher, M. J.; Durand, W. J.; Cushen, J. D.; Dean, L. M.; Blachut, G.; Ellison, C. J.; Willson, C. G. Polarity-Switching Top Coats Enable Orientation of Sub-10-nm Block Copolymer Domains. *Science* **2012**, *338*, 775−779.
(20) Durand, W. J.; Carlson, M. C.; Maher, M. J.; Blachut, G.; Santos, L. J.; Tein, S.; Ganesan, V.; Ellison, C. J.; Willson, C. G. Experimental and Modeling Study of Domain Orientation in Confined Block Copolymer Thin Films. *Macromolecules* **2016**, *49*, 308−316.
(21) Turner, M. S. Equilibrium Properties of a Diblock Copolymer Lamellar Phase Confined Between Flat Plates. *Phys. Rev. Lett.* **1992**, *69*, 1788−1791.
(22) Walton, D. G.; Kellogg, G. J.; Mayes, A. M.; Lambooy, P.; Russell, T. P. A Free Energy Model for Confined Diblock Copolymers. *Macromolecules* **1994**, *27*, 6225−6228.
(23) Bates, C. M.; Maher, M. J.; Janes, D. W.; Ellison, C. J.; Willson, C. G. Block Copolymer Lithography. *Macromolecules* **2014**, *47*, 2−12.
(24) Maher, M. J.; Bates, C. M.; Blachut, G.; Carlson, M. C.; Self, J. L.; Janes, D. W.; Durand, W. J.; Lane, A. P.; Ellison, C. J.; Willson, C. G. Photopatternable Interfaces for Block Copolymer Lithography. *ACS Macro Lett.* **2014**, *3*, 824−828.
(25) Lane, A. P.; Maher, M. J.; Willson, C. G.; Ellison, C. J. Photopatterning of Block Copolymer Thin Films. *ACS Macro Lett.* **2016**, *5*, 460−465.
(26) Koneripalli, N.; Singh, N.; Levicky, R.; Bates, F. S.; Gallagher, P. D.; Satija, S. K. Confined Block Copolymer Thin Films. *Macromolecules* **1995**, *28*, 2897−2904.
(27) Lambooy, P.; Russell, T.; Kellogg, G.; Mayes, A.; Gallagher, P.; Satija, S. Observed Frustration in Confined Block Copolymers. *Phys. Rev. Lett.* **1994**, *72*, 2899−2902.
(28) Andersen, T. H.; Tougaard, S.; Larsen, N. B.; Almdal, K.; Johannsen, I. Surface Morphology of PS−PDMS Diblock Copolymer Films. *J. Electron Spectrosc. Relat. Phenom.* **2001**, *121*, 93−110.
(29) Maher, M. J.; Rettner, C. T.; Bates, C. M.; Blachut, G.; Carlson, M. C.; Durand, W. J.; Ellison, C. J.; Sanders, D. P.; Cheng, J. Y.; Willson, C. G. Directed Self-Assembly of Silicon-Containing Block Copolymer Thin Films. *ACS Appl. Mater. Interfaces* **2015**, *7*, 3323−3328.
(30) Jung, Y.-S.; Ross, C. A. Orientation-Controlled Self-Assembled Nanolithography Using a Polystyrene-Polydimethylsiloxane Block Copolymer. *Nano Lett.* **2007**, *7*, 2046−2050.
(31) Bita, I.; Yang, J. K. W.; Jung, Y.-S.; Ross, C. A.; Thomas, E. L.; Berggren, K. K. Graphoepitaxy of Self-Assembled Block Copolymers on Two-Dimensional Periodic Patterned Templates. *Science* **2008**, *321*, 939−943.
(32) Cushen, J. D.; Wan, L.; Blachut, G.; Maher, M. J.; Albrecht, T. R.; Ellison, C. J.; Willson, C. G.; Ruiz, R. Double-Patterned Sidewall Directed Self-Assembly and Pattern Transfer of Sub-10 nm PTMSS-*b*-PMOST. *ACS Appl. Mater. Interfaces* **2015**, *7*, 13476−13483.
(33) Fredrickson, G. H. *The Equilibrium Theory of Inhomogeneous Polymers*; Oxford University Press: Oxford, UK, 2006.
(34) Matsen, M. W. Self-Consistent Field Theory and Its Applications. In *Soft Matter, Vol. 1: Polymer Melts and Mixtures*; Gompper, G., Schick, M., Eds.; Wiley: Weinheim, Germany, 2006; pp 87−178.
(35) Silberberg, A. Distribution of Conformations and Chain Ends Near the Surface of a Melt of Linear Flexible Macromolecules. *J. Colloid Interface Sci.* **1982**, *90*, 86−91.

DOI: 10.1021/acsnano.6b05390
ACS Nano 2016, 10, 10152−10160

Supporting Information for Structure, Stability, and Reorganization of 0.5 L_0 Topography in Block Copolymer Thin Films

Michael J. Maher,[1,5‡] Jeffrey L. Self,[3‡] Pawel Stasiak,[4‡] Gregory Blachut,[2] Christopher J. Ellison,[2,5] Mark W. Matsen,[6*] Christopher M. Bates,[7,8*] and C. Grant Willson[1,2*]

[1]Department of Chemistry and the [2]McKetta Department of Chemical Engineering, The University of Texas at Austin, Austin, TX 78712

[3]Department of Chemistry, University of California, Santa Barbara, Santa Barbara, CA 93106.

[4]Department of Mathematics & Statistics, University of Reading, Reading, U.K.

[5]Department of Chemical Engineering and Materials Science, University of Minnesota, Minneapolis, MN 55455

[6]Department of Chemical Engineering, Department of Physics & Astronomy, Waterloo Institute for Nanotechnology, University of Waterloo, Waterloo, Ontario, Canada

[7]Materials Department and [8]Department of Chemical Engineering, University of California, Santa Barbara, Santa Barbara, CA 93106.

* To whom correspondence should be addressed: willson@che.utexas.edu, bates@engr.ucsb.edu, mwmatsen@uwaterloo.ca, cellison@umn.edu

‡ Denotes equal contributions

Instrumentation

Ellipsometry was performed with a J.A. Woollam Co, Inc. VB 400 VASE Ellipsometer using wavelengths from 382 to 984 nm and a 65° angle of incidence. Optical micrographs were collected on an Olympus BX60 equipped with a Spot Insight QE Model 4.2 camera. AFM data was collected on an Asylum MFP-3D Origin using NanoWorld Pointprobe (NCH, resonance frequency = 320 kHz, force constant = 42 N/m) tips. Scanning electron microscopy samples were cross-sectioned and briefly etched using a Plasma-Therm Versaline. The following etch recipe was used: pressure= 6 mTorr, RF1 power = 20 W, RF2 power = 100 W, O_2 flow rate = 20 scmm, temperature = 20˚C. The samples were subsequently coated in gold/palladium using an Emitech K550X at 20 mA for 10 sec prior to imaging. Scanning electron micrographs were taken on a Leo 1550 using an accelerating voltage of 10 kV. Brightness and contrast on all SEMs were uniformly enhanced using commercial image editing software.

Reagents and Materials

MIBK and methanol were purchased from Sigma-Aldrich. Test-grade silicon wafers (100) were purchased from Silicon Quest International. All reagents were used without further purification unless stated. The synthesis of the block copolymer, PS-PTMSS, and top coats can be found elsewhere.[1]

Cross-section SEM Samples for Figure 1

Thick BCP samples utilized for cross section SEM were generated with two boundary conditions: (1) a neutral (or near neutral) polymer that chemically looks like a top coat but is instead grafted to the substrate surface combined with a free surface, or (2) SiO_2 at the substrate surface and the aforementioned top coat now applied as an actual top coat. The grafting procedure and materials have been previously reported in full.[2] The grafted surface treatment polymer contains 50 mol% maleic anhydride and 50 mol% 4-*tert*-butoxystyrene. After grafting, the surface was ≈3 nm thick. Island and hole formation using PS-PTMSS was the same as described above. All SEM samples were annealed at 180˚C for 10 min, cross-sectioned, etched, and coated in gold/palladium prior to imaging. The top coat in situation (2) was not removed prior to imaging.

Cross-linked Blends for Figure 3

Two different cross-linkable surface treatments (containing 48 mol% and 65 mol% PtBS, respectively) were blended by mass to produce different molar ratios of PtBS:PMMA (PVBzAz was assumed to be constant). After cross-linking as previously described, PS-PTMSS was spin coated to achieve an as-cast film thickness of 1.65 L_0. The samples were annealed at 180˚C and imaged by optical microscope at various times.

Surfaces Corresponding to Figures 4–7

Slightly Asymmetric Wetting Conditions

The substrate surface was poly(4-*tert*-butylstyrene-*random*-methylmethacrylate-*random*-4-vinylbenzylazide) (XST-53) containing 53 mol% 4-tert-butylstyrene, 42 mol% methylmethacrylate, and 5 mol% 4-vinylbenzylazide, which is near neutral.[1] A 0.5 wt% solution of the polymer in toluene was spin coated onto a silicon wafer at 3000 rpm and crosslinked at 250˚C for 5 min on a hot plate. Un-crosslinked material (<1 nm) was removed by rinsing the silicon wafer with THF. The resulting film thickness was ≈10 nm. A solution of PS-PTMSS (0.8–2 wt% in MIBK) was spin coated onto the cross-linked surface between 1000–3500 rpm to achieve the desired film thickness. Samples were annealed at 180˚C for various amounts of time.

Slightly Symmetric Wetting Conditions

The preferential substrate surface was poly(styrene-*random*-4-vinylbenzylazide) containing 95 mol% PS, 5 mol% PVBzAz[1] crosslinked in the same fashion as the neutral analogue described above. The near neutral top coat contained 50 mol% maleic anhydride, 20 mol% 3,5-di-*tert*-butylstyrene, and 30 mol% styrene. The top coat was spin coated directly onto the BCP as the trimethylammonium salt, which is described in detail in a previous report.[1] Samples were annealed at 180˚C for various amounts of time.

Supplemental data

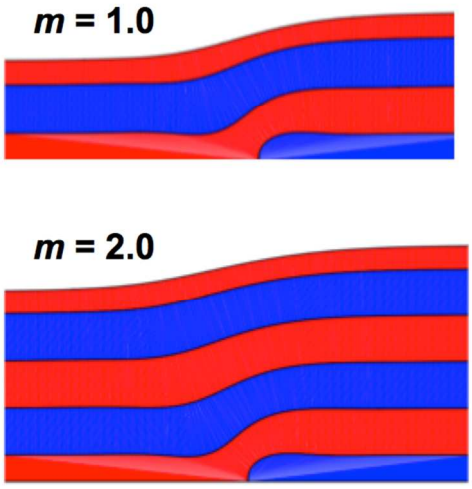

Figure S1. Additional simulated step edges between films with m and m + 0.5 lamellae (i.e., 0.5 L_0 topography) generated with f_A = 0.5 using a neutral substrate surface and preferential top surface; c.f., Figure 1.

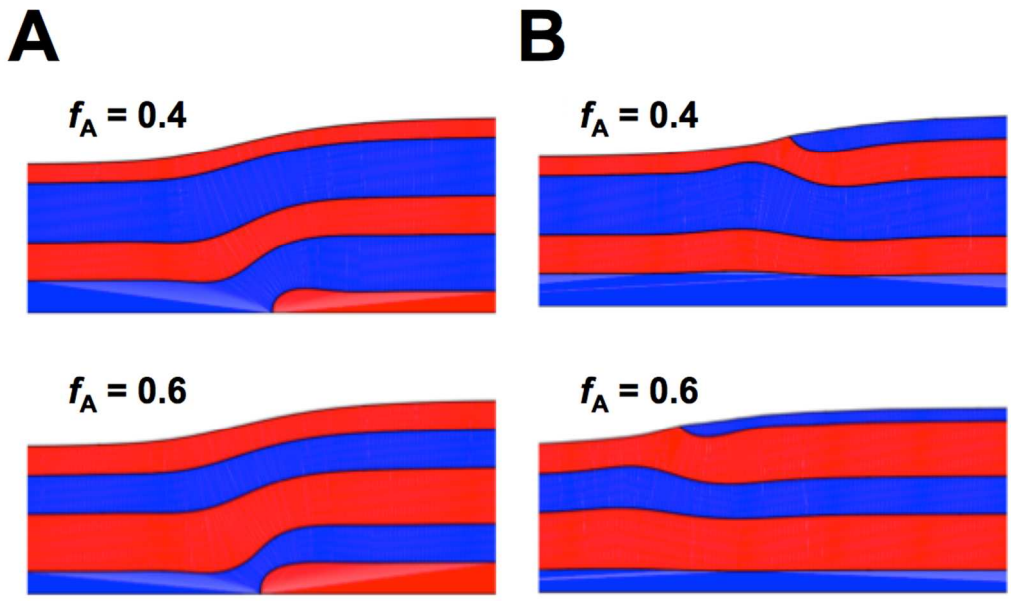

Figure S2. Additional simulated step edges between films with m = 1.5 and m + 0.5 lamellae (i.e., 0.5 L_0 topography) generated with various f_A using (A) a neutral substrate surface and preferential top surface and (B) a preferential bottom surface and neutral top surface; c.f., Figure 1.

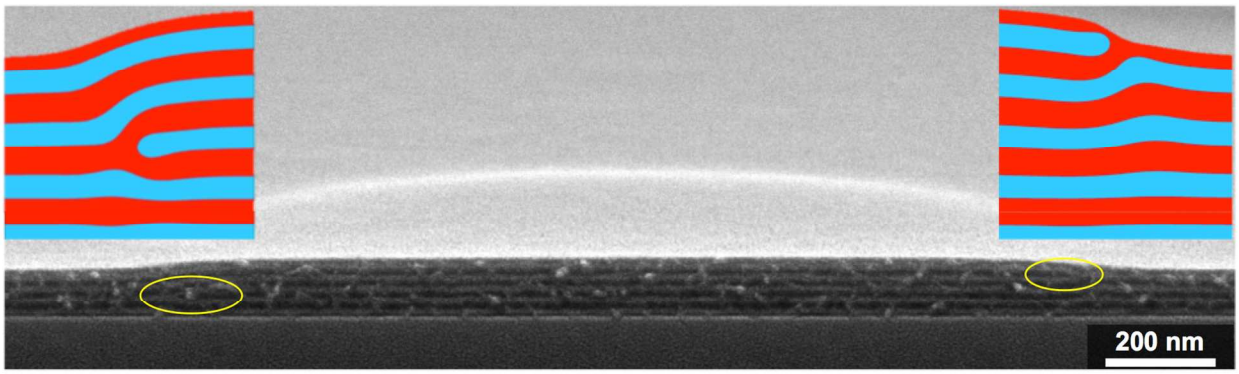

Figure S3. Cross-section SEM of a 1 L_0 island produced using PS-PTMSS annealed on SiO_2 (PS-preferential) with air as the free surface (PTMSS-preferential). The 0.25 L_0 PS substrate wetting layer (dark stripe) is difficult to distinguish. Edge dislocations can be seen in two different layers as depicted in the insets (adapted from Stasiak et al.). Note these are illustrations and not simulated structures. PTMSS is represented as red and PS blue.

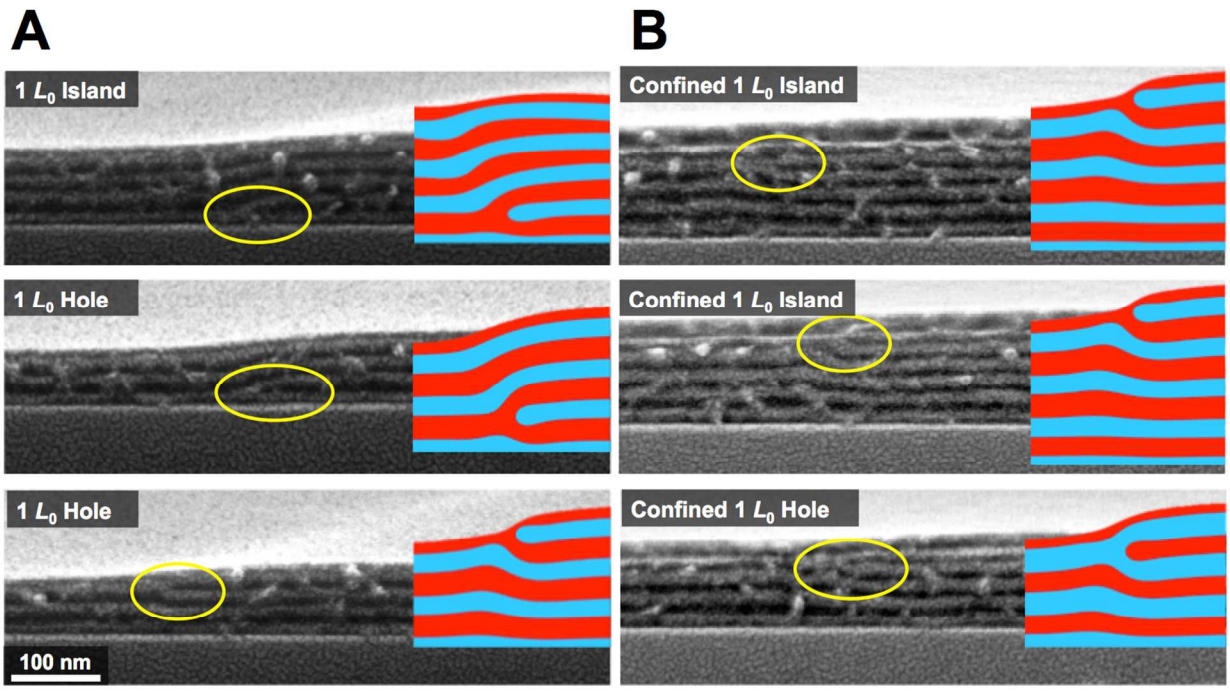

Figure S4. Asymmetric wetting cross section SEMs produced using PS-PTMSS annealed on SiO_2 (PS-preferential) with **A)** air as the free surface (PTMSS-preferential) and **B)** a PTMSS-preferential top coat. The 0.25 L_0 PS substrate wetting layer (dark stripe) is difficult to distinguish in most images. Note: Illustrations (not simulations) have been superimposed on the SEM images to help distinguish the dislocation position. PTMSS is represented as red and PS blue.

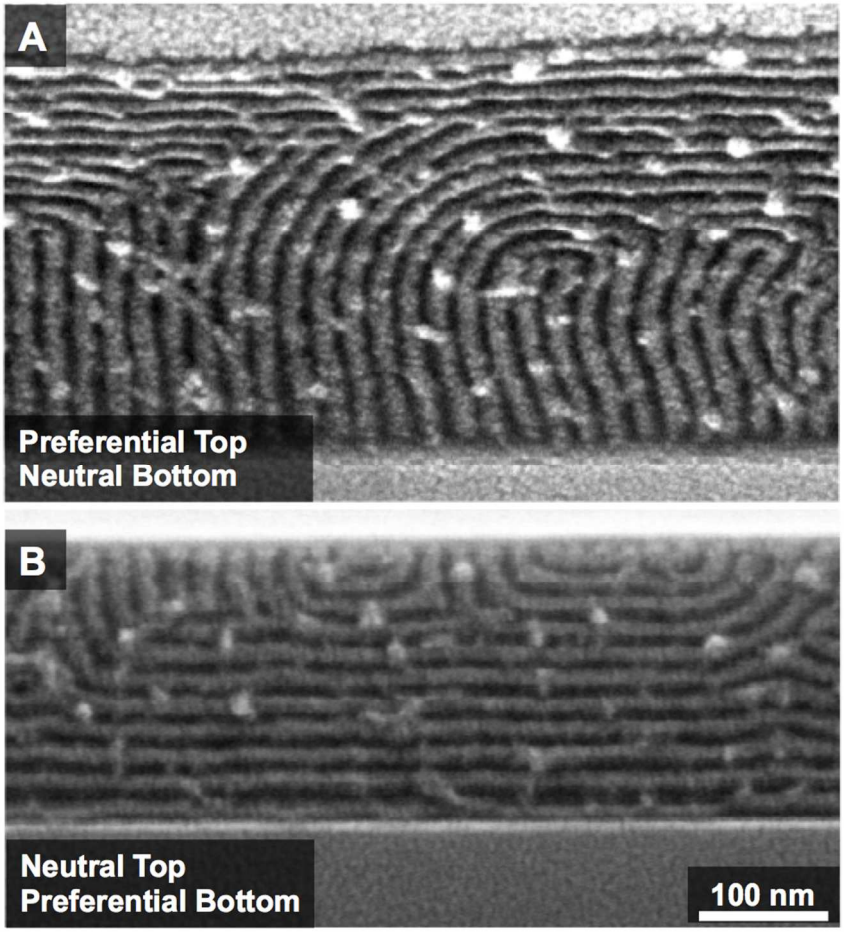

Figure S5. Cross section SEMs of thick BCP films with one neutral and one preferential surface. **A)** Near-neutral bottom surface (polymeric) with a free surface (air). **B)** Preferential bottom surface (polymeric) and near-neutral top coat.

Nucleation of 0.5 L_0 versus 1 L_0 islands

Here we consider the kinetics of 0.5 L_0 and 1 L_0 island formation, which occur when the initial film thickness is slightly larger than the preferred thickness by some amount ΔL. We assume that the film initially creates horizontal lamellae free of defects but with a slightly expanded period. Because the film needs to go through a first-order transition to change the number of layers[3] and there is no preferred location, islands should form by the classical homogeneous nucleation and growth mechanism.[4,5]

From the initial homogeneous state, we consider the spontaneous formation of a small circular nucleus of radius R consisting of an island of radius αR at the center surrounded by a terrace of the preferred film thickness (see Figure S6). The probability of this occurring is proportional to $\exp(-E/k_bT)$, where E is the energy of the nucleus. In order to grow, the nucleus has to overcome an energy barrier, E_B, by exceeding a critical radius,

R_c; otherwise, it will quickly vanish. Although our calculation is for island formation, the equations for hole formation are completely analogous.

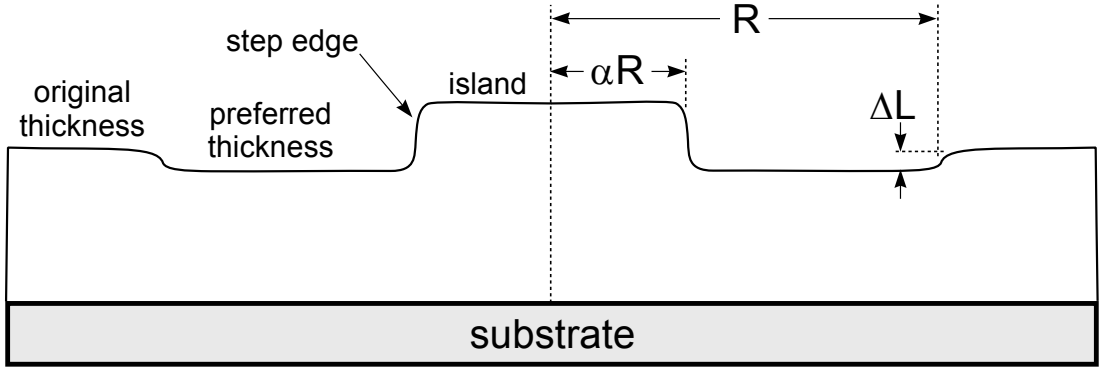

Figure S6. Cross-section of an island (1 L_0 or 0.5 L_0) nucleated from a homogeneous film that slightly exceeds the preferred thickness.

For 1 L_0 islands, the energy cost of forming a nucleus is

$$E_1 = -\pi R^2 \Delta f + 2\pi\alpha R\Gamma_1$$

where Δf is the excess free energy of the original film per unit area and Γ_1 is the line tension of a *1* L_0 step edge. Note that the line tension between the original film and the outer edge of the nucleus will be much smaller than Γ_1 since it does not involve a dislocation in the lamellae, and so we have neglected it. The maximum in E_1 with respect to R gives us the energy barrier,

$$E_{B,1} = \frac{\pi\alpha^2\Gamma_1^2}{\Delta f}$$

which occurs at the critical radius

$$R_{c,1} = \frac{\alpha\Gamma_1}{\Delta f}$$

Referring to Figure S6, conservation of material requires that the size of the island relative to the nucleus is

$$\alpha = \sqrt{\frac{\Delta L}{L_0}}$$

from which it follows that

$$E_{B,1} = \frac{\pi\Delta L\Gamma_1^2}{L_0\Delta f}$$

For 0.5 L_0 islands, the energy cost of forming a nucleus

$$E_{0.5} = -\pi R^2 \Delta f + \pi \alpha^2 R^2 \Delta\gamma + 2\pi\alpha R \Gamma_{0.5}$$

is the same as before except that the line tension of a 0.5 L_0 step edge, $\Gamma_{0.5}$, is smaller and there is an extra term involving a difference in surface tensions, $\Delta\gamma = \gamma_{\text{island}} - \gamma_{\text{film}}$. The latter accounts for the fact that a 0.5 L_0 island has a different component in contact with the *nearly* neutral surface than the rest of the film. Following the same reasoning as before, the energy barrier

$$E_{B,0.5} = \frac{\pi \alpha^2 \Gamma_{0.5}^2}{\Delta f \left(1 - \frac{\alpha^2 \Delta\gamma}{\Delta f}\right)}$$

occurs at a critical radius of

$$R_{c,0.5} = \frac{\alpha \Gamma_{0.5}}{\Delta f \left(1 - \frac{\alpha^2 \Delta\gamma}{\Delta f}\right)}$$

This time, conservation of material requires

$$\alpha = \sqrt{\frac{2\Delta L}{L_0}}$$

which implies that

$$E_{B,0.5} = \frac{2\pi \Delta L \Gamma_{0.5}^2}{L_0 \Delta f \left(1 - \frac{2\Delta L \Delta\gamma}{L_0 \Delta f}\right)}$$

We can now compare the relative heights of the two energy barriers

$$\frac{E_{B,0.5}}{E_{B,1}} = \frac{2\left(\frac{\Gamma_{0.5}}{\Gamma_1}\right)^2}{\left(1 - \frac{2\Delta L \Delta\gamma}{L_0 \Delta f}\right)}$$

Given our calculation of the line tensions which predicts $\Gamma_{0.5} \cong 0.3\Gamma_1$ and assuming a nearly neutral surface (i.e., $\Delta\gamma \cong 0$), the energy barrier for a 0.5 L_0 island is expected to be about 20% that of a 1 L_0 island. Since the rate of island formation is proportional to the exponential of the energy barrier, the 0.5 L_0 islands should form with a much greater frequency than 1 L_0 islands, even if they are slightly metastable.

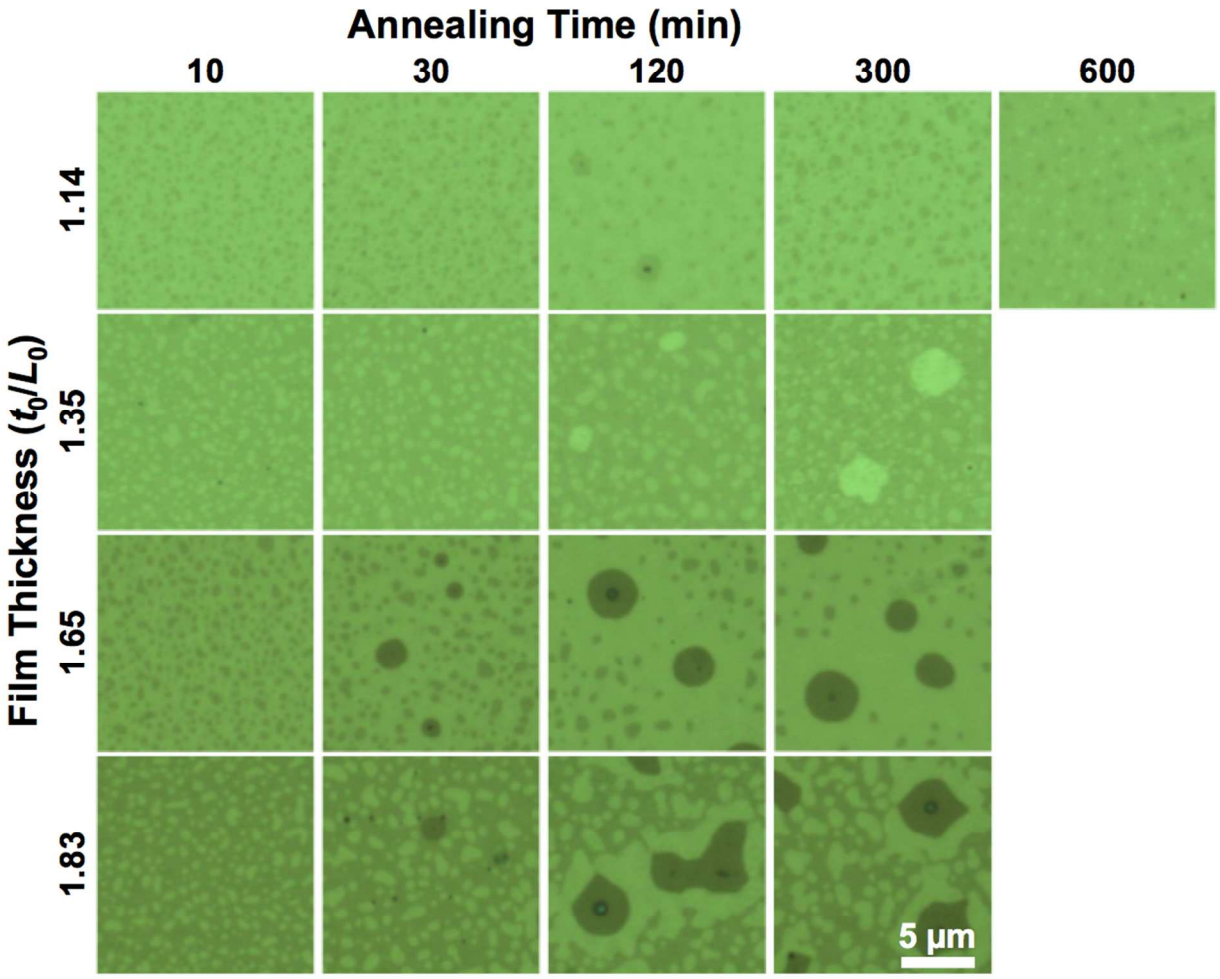

Figure S7. Optical micrographs of PS-PTMSS films annealed at 180˚C for various times between XST-53 and a free surface. The scale bar is valid for all micrographs.

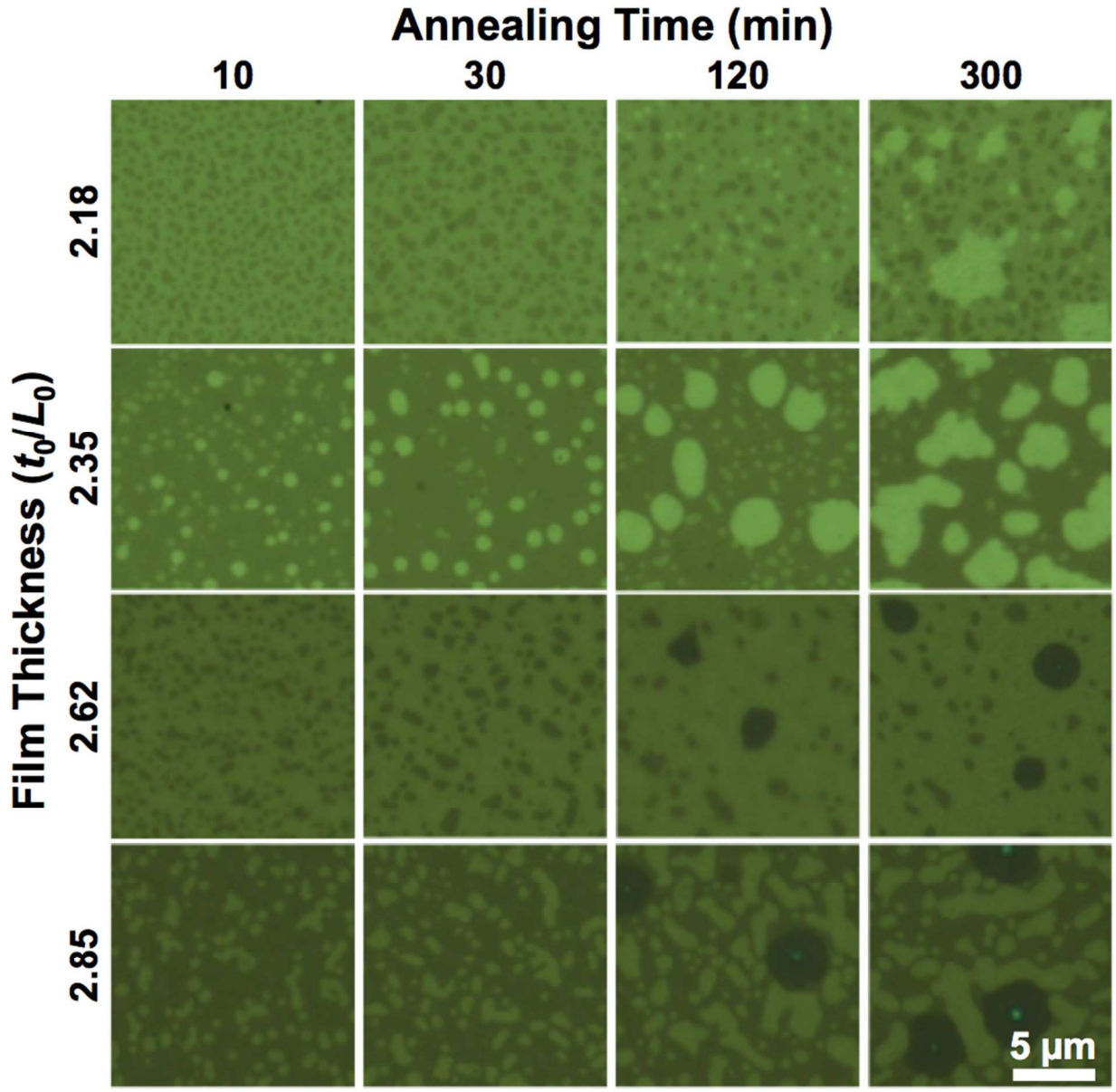

Figure S8. Optical micrographs of PS-PTMSS films annealed at 180˚C for various times between XST-53 and a free surface. The scale bar is valid for all micrographs.

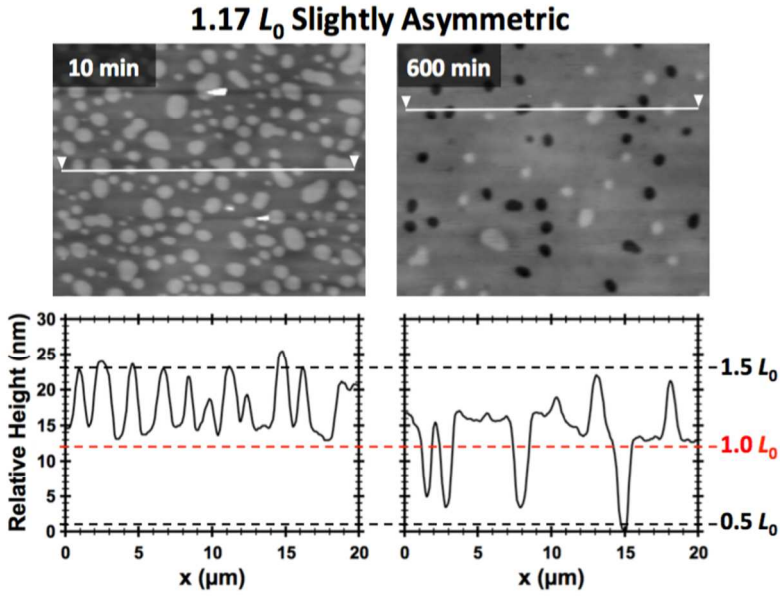

Figure S9. Atomic force micrographs of 1.17 L_0 thick PS-PTMSS annealed between XST-53 (substrate) and a free surface (top) at 180˚C for 10 and 600 min.

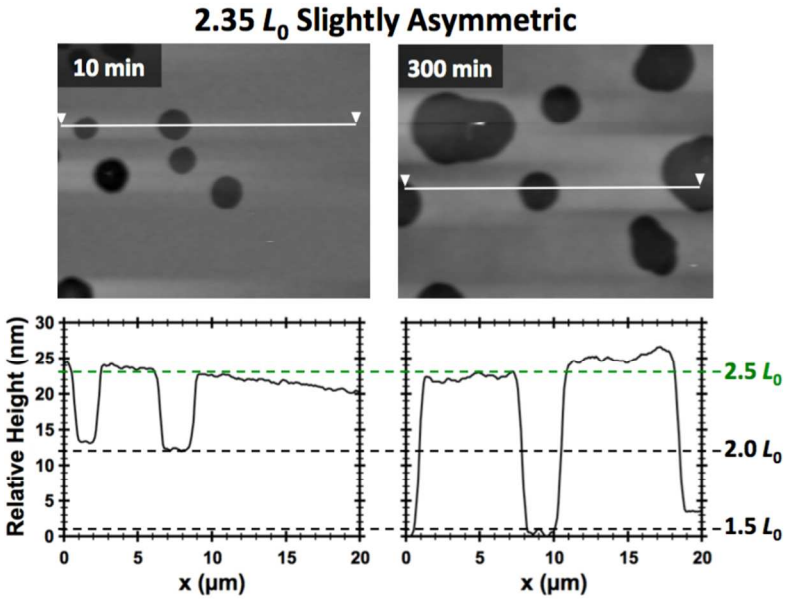

Figure S10. Atomic force micrographs of 2.35 L_0 thick PS-PTMSS annealed between XST-53 (substrate) and a free surface (top) at 180˚C for 10 and 300 min.

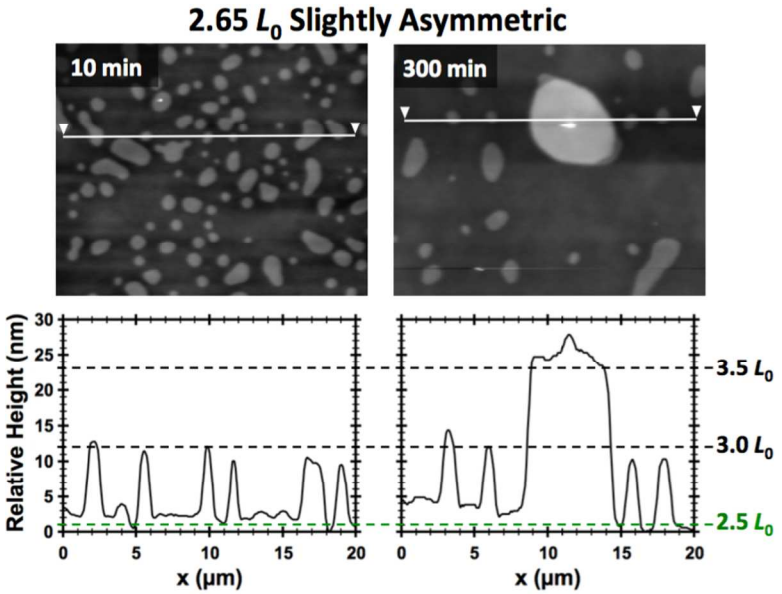

Figure S11. Atomic force micrographs of 2.65 L_0 thick PS-PTMSS annealed between XST-53 (substrate) and a free surface (top) at 180˚C for 10 and 300 min.

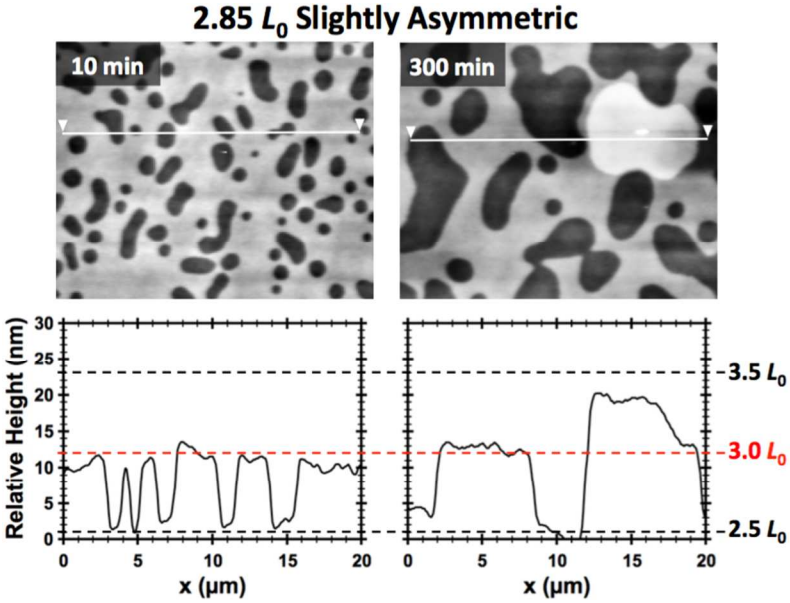

Figure S12. Atomic force micrographs of 2.85 L_0 thick PS-PTMSS annealed between XST-53 (substrate) and a free surface (top) at 180˚C for 10 and 300 min.

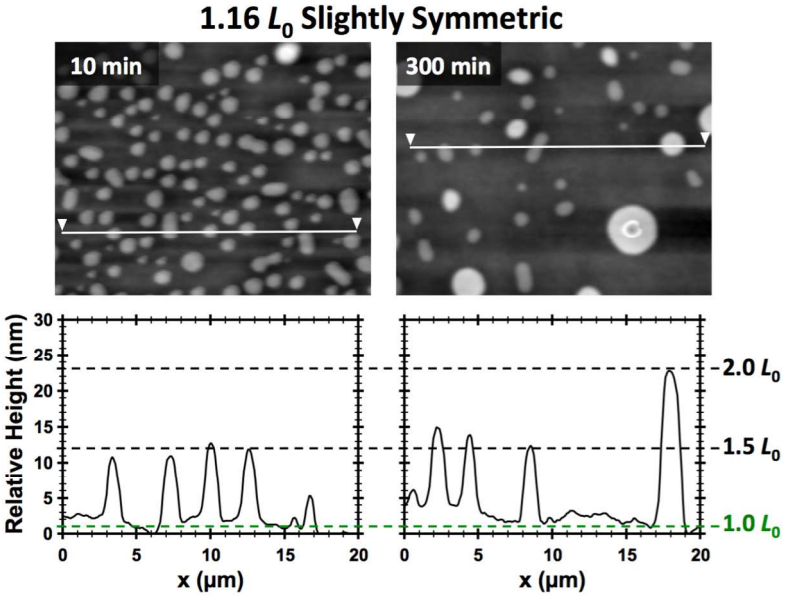

Figure S13. Atomic force micrographs of 1.16 L_0 thick PS-PTMSS annealed between cross-linked PS and a near-neutral top coat at 180˚C for 10 and 300 min.

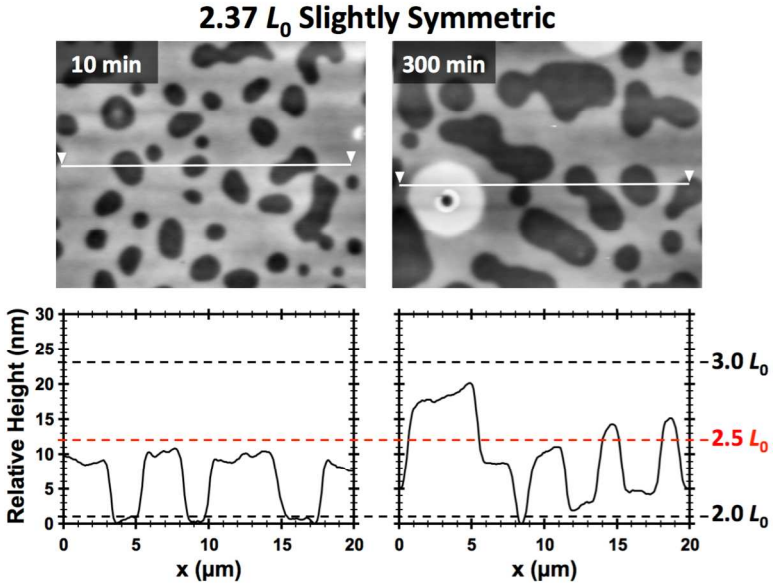

Figure S14. Atomic force micrographs of 2.37 L_0 thick PS-PTMSS annealed between cross-linked PS and a near-neutral top coat at 180˚C for 10 and 300 min.

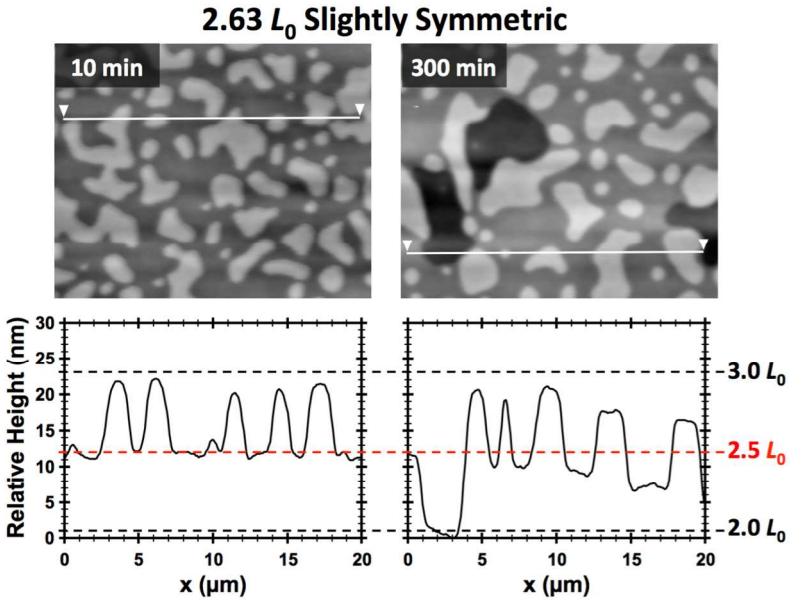

Figure S15. Atomic force micrographs of 2.63 L_0 thick PS-PTMSS annealed between cross-linked PS and a near-neutral top coat at 180˚C for 10 and 300 min.

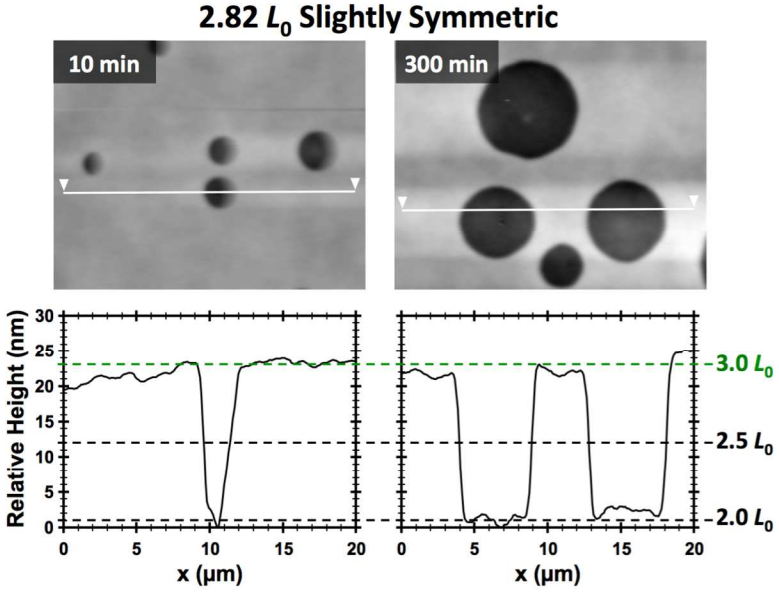

Figure S16. Atomic force micrographs of 2.82 L_0 thick PS-PTMSS annealed between cross-linked PS and a near-neutral top coat at 180˚C for 10 and 300 min.

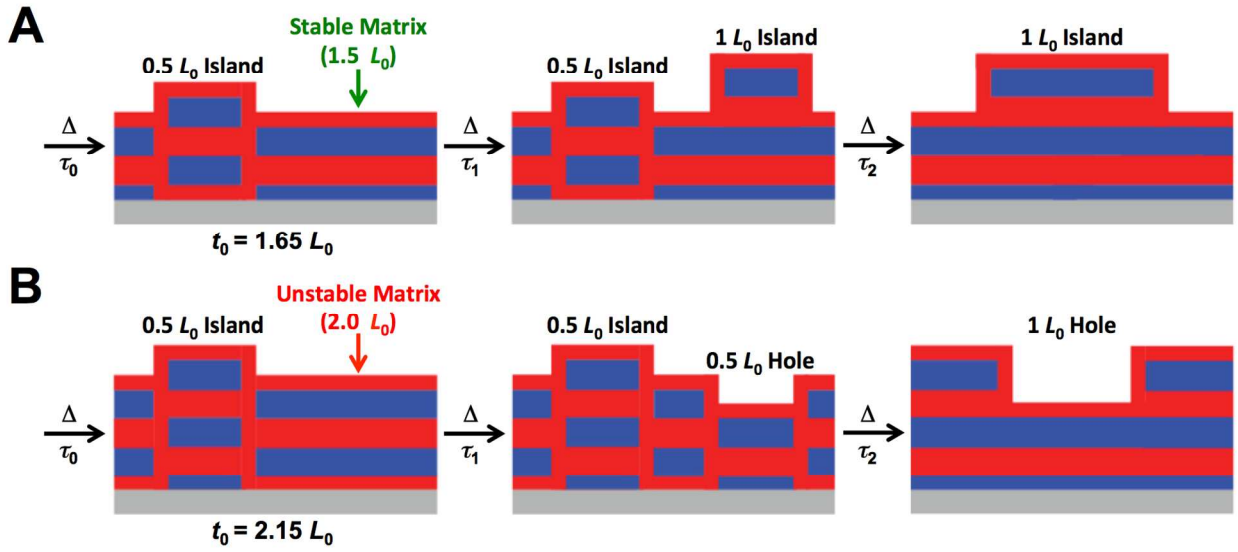

Figure S17. Illustration of surface reconstruction as a function of time for unconfined films with as-cast thickness **A)** t_0 = 1.65 L_0 and **B)** t_0 = 2.15 L_0. No attempt was made to realistically draw the through-film interface.

References

(1) Maher, M. J.; Bates, C. M.; Blachut, G.; Sirard, S.; Self, J. L.; Carlson, M. C.; Dean, L. M.; Cushen, J. D.; Durand, W. J.; Hayes, C. O.; Ellison, C. J.; Willson, C. G. Interfacial Design for Block Copolymer Thin Films. *Chem. Mater.* **2014**, *26*, 1471–1479.

(2) Maher, M. J.; Bates, C. M.; Blachut, G.; Carlson, M. C.; Self, J. L.; Janes, D. W.; Durand, W. J.; Lane, A. P.; Ellison, C. J.; Willson, C. G. Photopatternable Interfaces for Block Copolymer Lithography. *ACS Macro Lett.* **2014**, *3*, 824–828.

(3) Matsen, M. W. Thin Films of Block Copolymer. *J. Chem. Phys.* **1997**, *106*, 7781–7791.

(4) Strobl, G. R. *The Physics of Polymers*; Springer: Berlin, 2007.

(5) Jones, R. A. L. *Soft Condensed Matter*; Oxford University Press: Oxford, 2002.